Received: 15 December 2025 | Revised: 17 February 2026 | Accepted: 23 February 2026

DOI: 10.1002/suco.70546

ARTICLE

fib CEB-FIP WILEY

Failure mechanism and resistance predictions for one-way slabs in transition between shear and punching coupling linear elastic finite element analyses with critical shear crack theory-based models

Alex Micael Dantas de Sousa[1] | **Eva Olivia Leontien Lantsoght**[2,3] | **Andri Setiawan**[4] | **Mounir Khalil El Debs**[5]

[1]School of Engineering, São Paulo State University (UNESP), Ilha Solteira, Brazil

[2]Universidad San Francisco de Quito, Quito, Ecuador

[3]Delft University of Technology, Delft, The Netherlands

[4]Universitat Politècnica de València, Valencia, Spain

[5]São Carlos School of Engineering, University of São Paulo, São Carlos, Brazil

Correspondence
Alex Micael Dantas de Sousa, School of Engineering, São Paulo State University (UNESP), Ilha Solteira, Brazil.
Email: alex.dantas@unesp.br

Funding information
Fundação de Amparo à Pesquisa do Estado de São Paulo, Grant/Award Number: 2024/13561-5; Universidade Estadual Paulista, Grant/Award Number: EDITAL 03/2025 PROPe; Coordenação de Aperfeiçoamento de Pessoal de Nível Superior, Grant/Award Numbers: Finance Code 001, 00x0ma614

Abstract

Linear elastic finite element analyses (LEFEAs) have become more frequent in the design and assessment of reinforced concrete slabs under concentrated loads, as they enable low-cost evaluation of the distribution of shear forces over critical sections. However, few publications have addressed the benefits of combining LEFEA with mechanical-based models to predict the most critical shear failure mechanism and the corresponding shear and punching capacities. Notably, most previous studies employed a similar approach for a specific boundary condition or evaluated only the one-way shear capacity of slabs under concentrated loads near line supports. This study investigates the accuracy of the expressions based on the critical shear crack theory (CSCT) combined with LEFEA to assess the shear and punching capacity of one-way slabs under concentrated loads. Since such slabs may develop different failure mechanisms, this study also evaluates the level of accuracy to predict the governing shear failure mechanism identified in the tests, a topic rarely discussed until now. For this purpose, a dataset of 112 experiments was selected, covering different boundary conditions and loading arrangements. LEFEA was used to evaluate the uneven distribution of shear forces and bending moments on the critical shear regions. Some outputs from LEFEA were used in the analytical calculations with the CSCT-based expressions to predict the shear and punching capacity of such tests. The use of LEFEA also aided in understanding the change of shear failure mechanisms according to parameters such as the

member width to load size ratio b_{slab}/l_{load} and the shear slenderness a_v/d_l. The combination of the CSCT expressions with the LEFEA allows for predicting the governing shear failure mechanism and the shear capacity of the slabs for most tests accurately at a low computation cost. When the governing failure mechanism was not correctly identified, a conservative estimate of the shear capacity was provided, which is desirable in such cases.

KEYWORDS

critical shear crack theory, linear elastic finite element analysis, one-way shear, punching shear

1 | INTRODUCTION

Reinforced concrete one-way slabs under concentrated loads are commonly found in bridge deck slabs. These slabs are subjected to large concentrated loads in non-symmetrical loading and support conditions. Because of this, these members may show a transitional or asymmetrical shear failure mode between one-way shear (as wide beams [WBs] on slab strips) and two-way shear (punching shear), besides the flexural mechanisms.[1–3] Therefore, the assessment of such structures involves the evaluation of different (shear) failure mechanisms.[4] For design, it is usually not important which of the shear failure modes is the most critical since the most critical failure mechanism governs the design. Conversely, this information deserves more attention for assessing existing structures because it can indicate which regions of the structure need to be strengthened, or which loading position is critical in a proof load test. Within this context, linear elastic finite element analysis (LEFEA) stands out as an alternative to determining a more realistic distribution of shear forces and bending moments on relevant sections compared to pure analytical methods.

Despite the increasing number of studies developed with examples of the application of LEFEA to assess the shear capacity of one-way slabs under concentrated loads,[5–8] most of them present one or more of the following limitations:

i. The studies did not address how to combine LEFEA with mechanical-based shear and punching strength models. Most authors applied LEFEA only combined with semi-empirical code expressions.[5,7,9]
ii. When mechanical-based models were used to estimate the ultimate capacity of cantilever slabs, only the one-way shear resistance was checked.[1,6] In other words, it was assumed that one-way shear failures always governed for such slabs, and the possibility of punching failures was neglected.
iii. When shear and punching failure modes were investigated, a limited number of test results were addressed (between 1 and 3 experiments only), which limits the discussion about the level of accuracy of such approaches.[4,9]
iv. Slabs with continuity over the support were not discussed when applying the combination of LEFEA with mechanical-based models of the shear and punching capacity.[10]
v. The transition between one-way and two-way shear failures is usually not discussed based on the distribution of shear and bending moments, which limits the understanding of the interpretation of the test results.[5,11–13]

In this study, we investigate the accuracy of the approach first proposed by Natário,[10] which combines LEFEA with critical shear crack theory (CSCT) expressions to determine the shear and punching shear capacities of one-way slabs under concentrated loads. Compared to previous publications,[1,6] this study covers a higher variety of support conditions, which includes (i) one-way simply supported slabs (SSs), (ii) one-way slabs with continuity over one of the supports and (iii) cantilever members (Figure 1). Besides, this study discusses the transition between one-way and two-way shear failures for slabs under concentrated loads with different support conditions. Based on identifying key parameters for determining the governing failure mechanism between one-way shear and two-way shear, enhancements in Natário's approach[10] are performed mainly in the punching shear calculation method to consider parameters related to the transition between one-way shear and two-way shear.[12] These enhancements yield more precise predictions of the ultimate load, regardless of the governing failure mechanism. In other words, the ultimate load predicted with the punching shear expression, for instance, can be closer to the experimental load even if

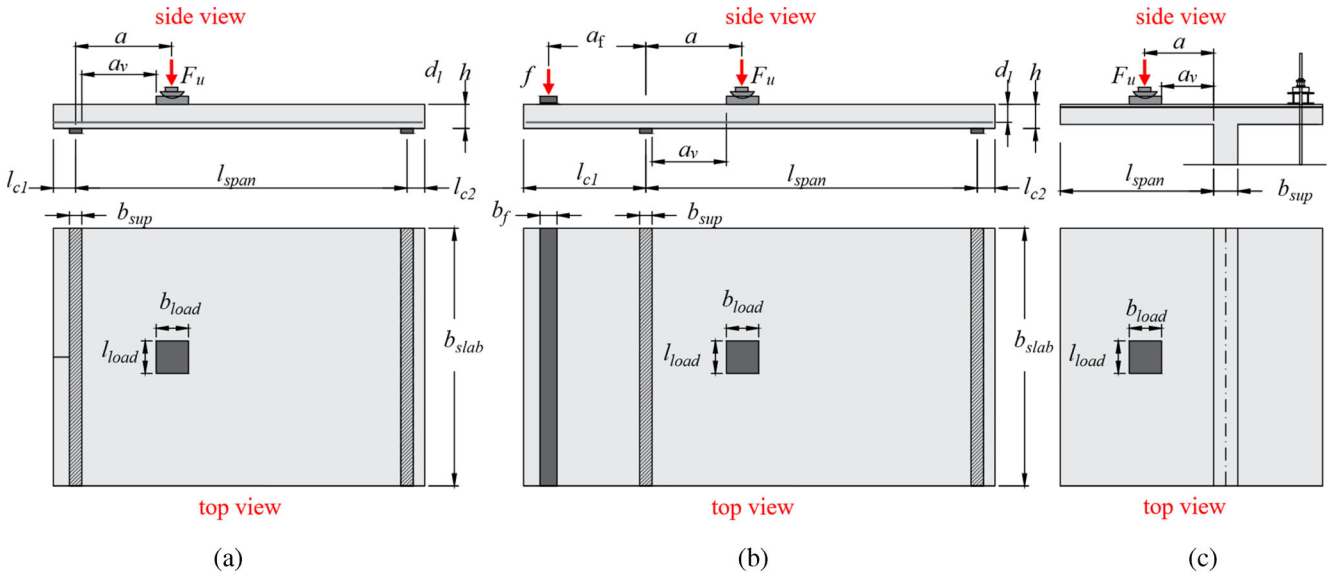

FIGURE 1 Sketch of one-way slabs under concentrated load: (a) simply supported slabs; (b) slabs with continuity on one of the supports (herein defined as continuous slabs) and (c) cantilever slabs.

the test failed by one-way shear instead of punching. As such, the robustness of the proposed methodology is improved.

In this paper, we first explain how to combine LEFEAs—using shell elements for the slabs—and the CSCT expressions of one-way[14] and two-way shear[15] to predict the shear and punching shear capacity of experiments available in the literature (Section 2). After (Section 3), we discuss the transition from one-way shear failures to two-way shear failures using a small set of experiments from the literature according to the CSCT expressions and information gathered from LEFEA. The Database of test results is described in Section 4. In the end (Section 5), comparisons between tested and predicted resistances are provided for the evaluated dataset, according to the boundary conditions of the tests and governing failure mechanism.

2 | BACKGROUND

2.1 | One-way shear capacity predictions using CSCT expressions and LEFEA

The one-way shear capacity $V_{R,\mathrm{CSCT}}$ of one-way slabs under concentrated loads was calculated according to Natário et al.[1] by combining the predicted unitary shear strength $v_{R,\mathrm{shear}}$ with an effective shear width b_{eff} (derived from LEFEA), and accounting for arching action in the one-way shear resistance for concentrated loads close to the support by β_{shear}:

$$V_{R,CSCT} = \frac{v_{R,shear} \cdot b_{eff}}{\beta_{shear}} \quad (1)$$

The unitary one-way shear resistance $v_{R,\mathrm{shear}}$ was calculated according to the CSCT expressions developed by Muttoni and Schwartz[16] and modified by Muttoni and Fernandez Ruiz.[14] The principle of this theory is that the flexural shear strength is governed by a flexural crack that develops diagonally (the critical shear crack) and disturbs the shear transfer actions. The main shear transfer mechanisms of slender beams, according to the CSCT, are[14]: (i) compression chord capacity or cantilever action,[17] (ii) aggregate interlock[18] and (iii) dowel action.[19,20] According to this model, the one-way shear capacity $v_{R,\mathrm{shear}}$ depends on the sectional geometry, the concrete compressive strength, the critical shear crack width w_{cr}, and the crack's roughness. The roughness is assumed as related to the aggregate size d_g,[21] while the crack width w_{cr} is assumed to be proportional to the reference longitudinal strain ε times the effective depth of the member d_l. In this way, the unitary shear capacity $v_{R,\mathrm{shear}}$ or failure criterion is calculated as (SI units: f_c in MPa; d_g in mm):

$$v_{R,shear} = \frac{d_l \cdot \sqrt{f_c}}{3} \cdot \frac{1}{1 + 120 \cdot \frac{\varepsilon \cdot d_l}{16 + d_g}} \quad (2)$$

where d_g is the measured maximum aggregate size if f_c <70 MPa and 0 mm if higher.

The reference longitudinal strain ε is evaluated at the control section at a depth of $0.6d_l$ from the compression face, assuming that plane sections remain plane and neglecting the tensile strength of the concrete (which is assumed to behave linearly elastically in compression). In the absence of normal forces, the reference strain ε at the control depth and height of the compression zone c_{flex} are given by[14] (SI units; d_l in m; m_{max} in kN/m):

$$\varepsilon = \frac{m_{max}}{b_w \cdot d_l \cdot \rho_l \cdot E_s \cdot \left(d_l - c_{flex}/3\right)} \cdot \frac{0.6 \cdot d_l - c_{flex}}{d_l - c_{flex}} \quad (3)$$

$$c_{flex} = d_l \cdot \rho_l \cdot \frac{E_s}{E_c} \cdot \left(\sqrt{1 + \frac{2 \cdot E_c}{\rho_l \cdot E_s}} - 1\right) \quad (4)$$

where m_{max} is the maximum bending moment at the control section for a given applied load, ρ_l is the flexural reinforcement ratio, E_c is the elastic modulus of the concrete, E_s is the elastic modulus of the steel, and c_{flex} is the height of the compression zone in the cross-section.

In this approach, the parameters that need to be evaluated in the numerical models are the distribution of unitary shear forces v (to calculate v_{avg} and b_{eff}), unitary bending moments m (to calculate m_{max}), and the total shear force going through the control section $V_{control}$ for a given applied load. Alternatively, $V_{control}$ can be directly determined from beam statics. Further details on the numerical models will be given in the next sections.

Evaluating the one-way slabs under concentrated loads, it is common to assume that only a slab strip, with a so-called effective shear width, contributes to the one-way shear capacity. Generally, the effective shear width is determined geometrically, assuming that the load spreads horizontally from the back sides of the loaded region toward the support with an angle of 45° (Figure 2a). However, this approach has the shortcoming that the predicted effective shear width increases too much as the distance from the load to the support increases. Someone may note that, in this approach, the predicted shear demand v_E comes from the assumed definition of the effective shear width (Figure 2a). In light of these limitations, Halvonik et al.[6] suggested limiting the spreading zone to $2d$ from the load frontal face, in such a way that the predicted effective shear width would increase only in the range $0 \leq a_v < 2d$. Nevertheless, this approach was validated only for cantilever slabs and requires further investigation to other support conditions.

Another definition is based on the uneven distribution of shear forces at the control section (Figure 2b). In this case, it is assumed that the effective shear width is defined as the length that, when multiplied by the maximum shear demand $v_{E,max}$, equals the shear force in that direction.[23] In the second option, the control shear demand $v_{E,max}$ comes from the measured shear demand distribution through LEFEA.

In this study, the effective shear width b_{eff} was calculated by dividing the total shear force in the full slab section of width b ($V_{control}$) by an averaged unitary shear force over the control sections v_{avg}[1,24] (Figure 2c) determined with a finite element model (Equation (5)). To be consistent with the CSCT principles, the control section to calculate the averaged unitary shear forces and the maximum bending moments is at $0.5d_l$ from the face of the load for simply SSs (Figure 3a) and $0.5d_l$ from the edge of the support on cantilever slabs (Figure 3b), on which d_l is effective depth toward the longitudinal reinforcement. The length of the control section (distribution

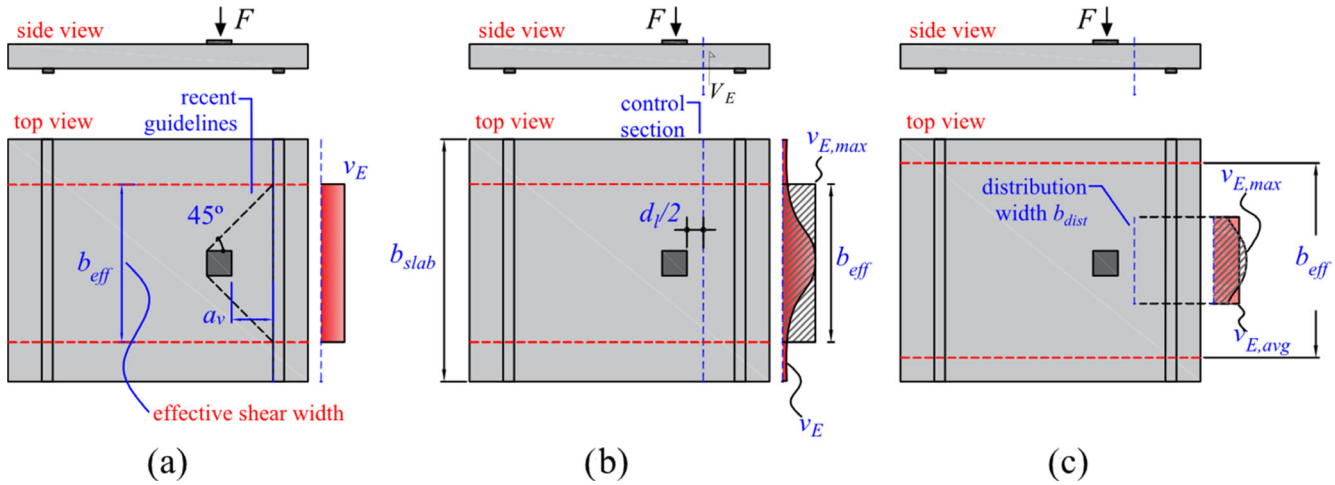

FIGURE 2 Definitions of effective shear width: (a) current French and Dutch approaches[22]; (b) definition based on the maximum unitary shear demand[23]; (c) definition based on the average shear demand over a distribution width.

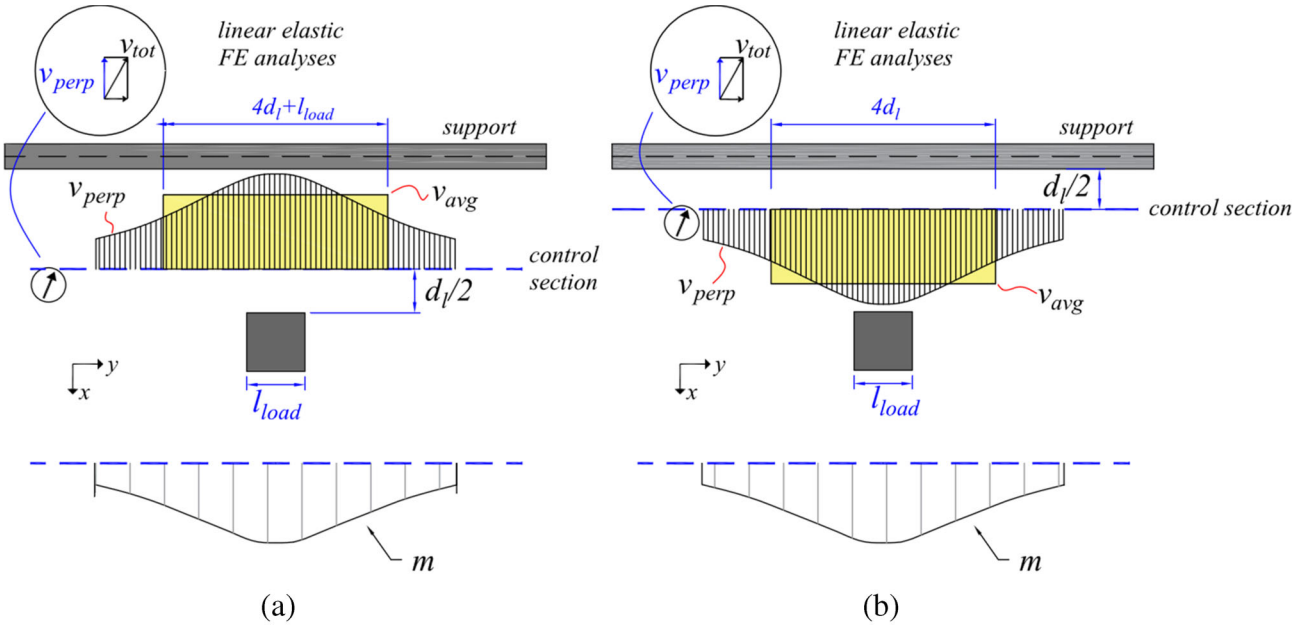

FIGURE 3 Control section location and averaged unitary shear force v_{avg} definition for (a) simply supported slabs and (b) cantilever slabs. Adapted from Natário.[10]

width) over which v is averaged to calculate v_{avg} is assumed $4d_l$ for cantilever slabs[25] and $4d_l + l_{load}$ for simply SSs (Figure 3).[10] For tests with continuity on one of the supports, it is necessary to examine if maximum bending moments occur close to the load or close to the support (depending on the degree of continuity and load layout). If the larger bending moment occurs close to the load, the verification follows the same principles as for simply SSs. On the other hand, the calculations follow the principles applied to cantilever slabs when the larger bending moment occurs close to the support.

Therefore, when combining LEFEA with the CSCT expressions, we firstly use a distribution width to calculate an average unitary shear force v_{avg} at the control section (perpendicular to the control section) and after the effective shear width b_{eff} is calculated as:

$$b_{eff} = \frac{V_{control}}{v_{avg}} \tag{5}$$

The arching action that takes place for loads close to the support, which increases the one-way shear resistance for such conditions, is accounted for by β_{shear}[10] (Equation (6)):

$$\beta_{shear} = \frac{a_v}{2.75 \cdot d_l}, \text{ with } d_l \le a_v \le 2.75 d_l \tag{6}$$

where a_v is the distance between faces of load and support (see Figure 1). Note that the CSCT was derived assuming flexural-shear failures and that the β_{shear} is only a simplification to allow estimating the enhanced resistance in the case of possible shear-compression failures. For slabs influenced by arching action (loads close to the support), using b_{eff} allows us to include the effect of the arching action in the load portion from F that is transferred directly to the support. Conversely, for slabs subjected to a load further away from the support, the use of b_{eff} could be suppressed. For such cases, one could simply compare the ultimate concentrated load F_{exp} with the calculated load that causes a one-way shear failure $F_{predicted}$.

Figure 4a shows the flowchart of calculations performed combining LEFEA output with the CSCT shear expressions. First, a unitary force $F_{hyp} = 1$ kN is applied to the numerical model to compute the averaged shear force $v_{avg,1kN}$, and the maximum bending moments $m_{max,1kN}$, over the control section. The self-weight was not considered in the numerical models as a simplification, since it was considerably lower than the applied concentrated loads at failure. Then, the effective shear width b_{eff} is calculated according to Equation (5) and Figure 3. In the end, a subroutine is used to find the applied concentrated load $F_{hyp,i}$, iteratively, which equals the unitary shear resistance $v_{R,i}$ with the average shear demand $v_{avg,i}$ over the control section (see Figure 4b). When the iterative process ends, the one-way shear capacity (in force units) V_R is calculated, accounting for the effective shear width b_{eff} and the arching action for loads close to the support (a_v <2.75 d_l). With this

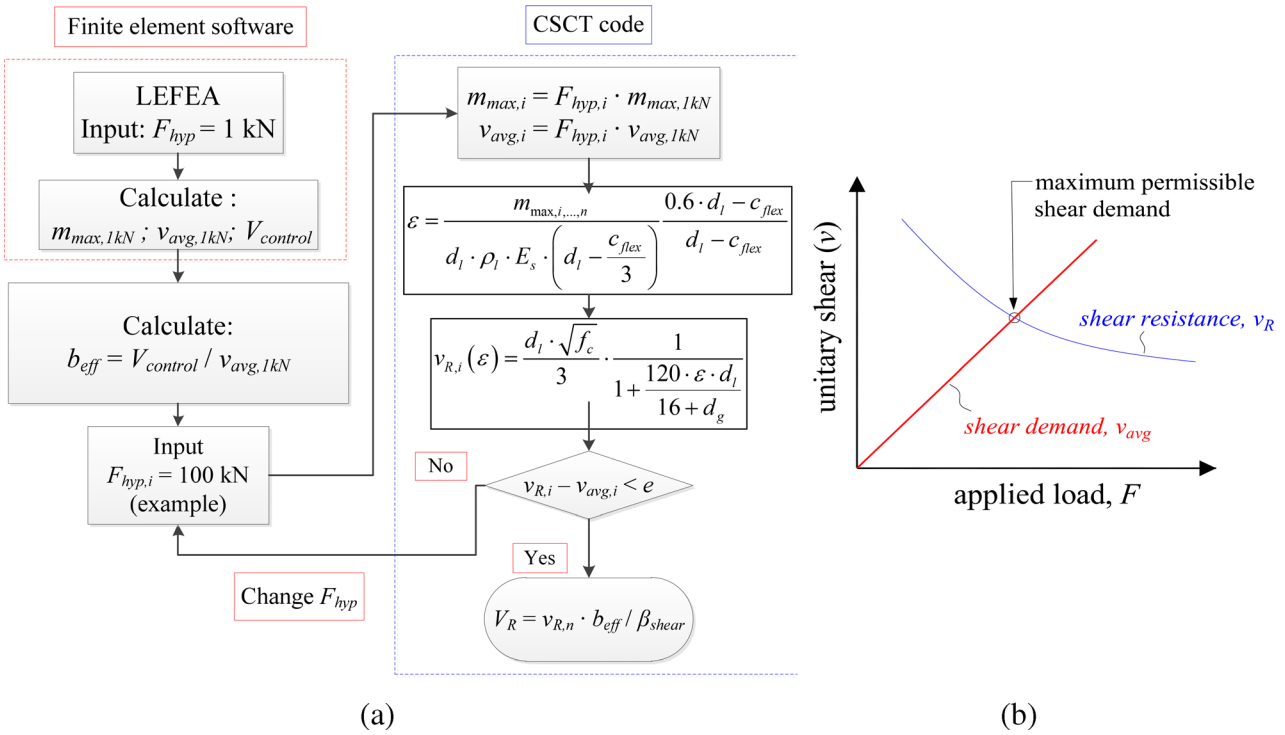

FIGURE 4 (a) Flowchart of the main steps for evaluating the one-way shear resistance following CSCT in combination with LEFEA; (b) Sketch of the iterative process combining the shear demand v_{avg} and shear resistance v_R (SI units). Adapted from.[26]

procedure, the externally applied load ($F_{predicted}$) that causes the sectional shear failure and the one-way shear resistance ($V_{R,CSCT}$) are predicted. $F_{predicted}$ is the last value of $F_{hyp,i}$ in the iterative process for which $v_{R.i}$ is equal to $v_{avg.i}$.

Since the relation between the applied load and the sectional shear force depends only on the load position and support layout, the comparison between tested and predicted resistances could be performed directly in terms of the applied concentrated loads in the tests F_{test} and the predicted value $F_{predicted}$. In other words, for loads that are not influenced by arching action, the comparison between the tested and predicted failure loads ($F_{test}/F_{predicted}$) equals the ratio between tested and predicted shear resistances ($V_{test}/V_{predicted}$). Therefore, for such cases, the calculation of the effective shear width would not be necessary. In this study, however, the effective shear width was calculated for all tests as a way to include the influence of arching action when applicable, as recommended by Natário.[10]

2.2 | Punching shear predictions aided by LEFEA

The punching shear capacity was evaluated using the CSCT ($\psi_x - \psi_y$) method[27,28] inspired by the work of Natário[10] with improvements as explained in this section. The control perimeter is placed at $d_v/2$ from the load edges, where d_v is the mean depth of the flexural reinforcement in both directions. The control perimeter is usually divided into four segments, assuming constant rotations $\psi_x - \psi_y$ and unitary strengths $v_{R.x} - v_{R.y}$ for each segment. The control perimeter with straight corners was adopted in this study to simplify the post-processing of the numerical results.

The punching shear strength is given by (assuming square loads or loads of limited rectangularity: $l_{load} \leq 3d_v$ and $b_{load} \leq 3d_v$):

$$P_{R,punching} = v_{R,x1} \cdot b_{0,x1} + v_{R,x2} \cdot b_{0,x2} + v_{R,y1} \cdot b_{0,y1} + v_{R,y2} \cdot b_{0,y2} \quad (7)$$

where the parts of the punching perimeter $b_{0.ij}$ are defined in Figure 5 (i refers to the directions evaluated, direction x or y, and j refers to the side of the control perimeter in the evaluated direction, sides 1 or 2).

The CSCT expressions for punching shear assume that increasing the width of the critical shear crack w_{cr} reduces the strength of the compression strut carrying shear around the loaded area.[16] The width of the critical shear crack w_{cr} is assumed proportional to the product between the slab rotation ψ and the effective depth of the

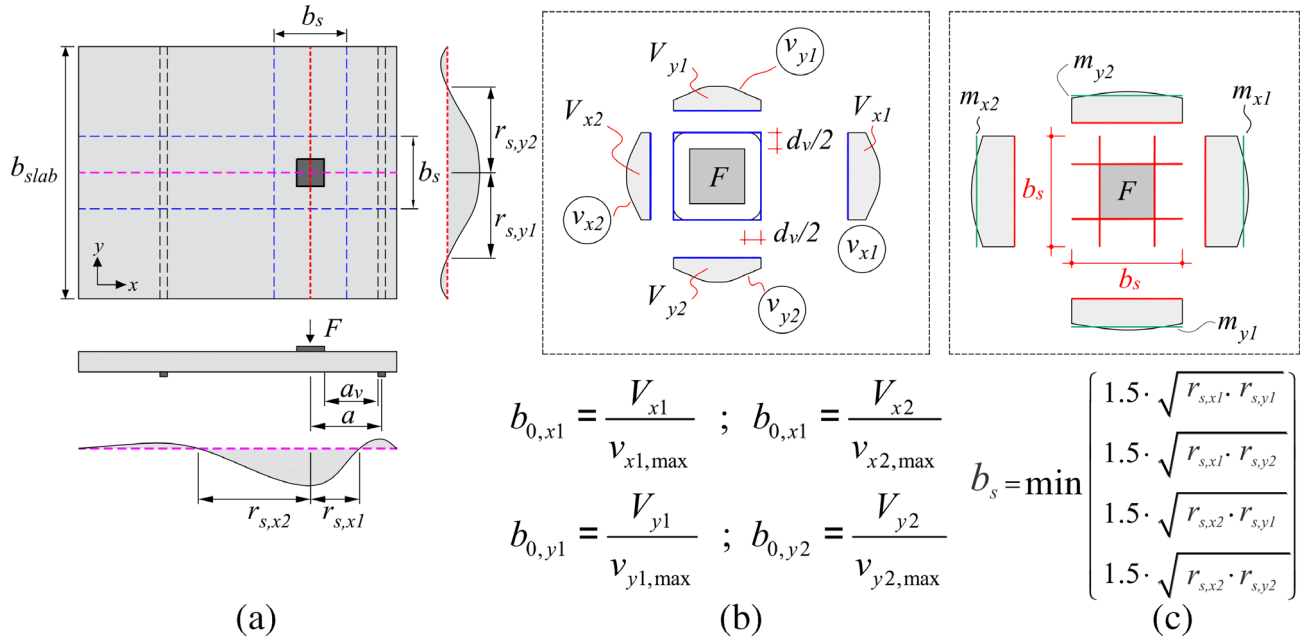

FIGURE 5 Definition of (a) $r_{s.ij}$ distances; (b) reduced control perimeters for square loads; and (c) averaged acting bending moments at the edges of the concentrated load and support strip widths. Adapted from Natário.[10]

reinforcement d_v,[15,16] where d_v is the average effective depth between longitudinal and transverse reinforcements. The CSCT also considers the shear redistribution around the loaded area in a simplified way. In this method, the slab rotations depend on the considered direction and are uneven along the control perimeter, meaning that some parts of the slab reach their ultimate strength while others still have a potential shear capacity.[10,27,28]

The unitary shear strength in each segment $v_{R.ij}$ is calculated as[29] (SI units: f_c in MPa; d_g in mm):

$$v_{R,ij} = \frac{(3/4) \cdot d_v \cdot \sqrt{f_c}}{1 + 15 \cdot \left[\psi_{ij} \cdot d_v / \left(d_g + d_{g0}\right)\right]} \tag{8}$$

$$d_{g0} = \begin{cases} 16\,\text{mm}, \text{if } f_c < 70MPa \\ 0\,\text{mm}, \text{if } f_c \geq 70MPa \end{cases} \tag{9}$$

where d_g is the maximum aggregate size and f_c the concrete compressive strength. The rotations ψ_{ij} in each side of the control perimeter were calculated according to level of approximation III from the *fib* Model Code provisions,[29] which are based on the CSCT.[15] In each segment of the control perimeter, the rotation was calculated as:

$$\psi_{ij} = 1.2 \cdot \frac{r_{s,ij}}{d_i} \cdot \frac{f_{yi}}{E_s} \cdot \left(\frac{m_{s,ij}}{m_{R,i}}\right)^{3/2} \tag{10}$$

$$\begin{aligned} m_{s,ij} &= \frac{1}{b_s} \cdot \int_{-b_s/2}^{+b_s/2} |m_{ij}| \cdot di \; i \perp j \\ m_{s,x1} &= \frac{1}{b_s} \cdot \int_{-b_s/2}^{+b_s/2} m_{x1} \cdot dy; \; m_{s,x2} = \frac{1}{b_s} \cdot \int_{-b_s/2}^{+b_s/2} m_{x2} \cdot dy; \\ m_{s,y1} &= \frac{1}{b_s} \cdot \int_{-b_s/2}^{+b_s/2} m_{y1} \cdot dx; \\ m_{s,y2} &= \frac{1}{b_s} \cdot \int_{-b_s/2}^{+b_s/2} m_{y,2} \cdot dx \end{aligned} \tag{11}$$

Natário[10] explains that $r_{s.ij}$ is the distance between maximum span moment due to concentrated load and the point of contraflexure (see Figure 5a), d_i is the effective flexural depth in the appropriate direction, f_{yi} is the steel yielding stress, E_s is Young's modulus of steel, $m_{s.ij}$ is the averaged acting bending moment at the loading plate edge ij within the width b_s (Figure 5c) and $m_{R.i}$ is the yielding moment per unit length in the evaluated direction. The support strip width b_s is calculated as:

$$b_s = \min\left\{1.5 \cdot \sqrt{r_{s,xj} \cdot r_{s,yj}}\right\} \tag{12}$$

The length of each segment of the control perimeter ($b_{0.x1}$, $b_{0.x2}$, $b_{0.y1}$ and $b_{0.y2}$), calculated without rounded

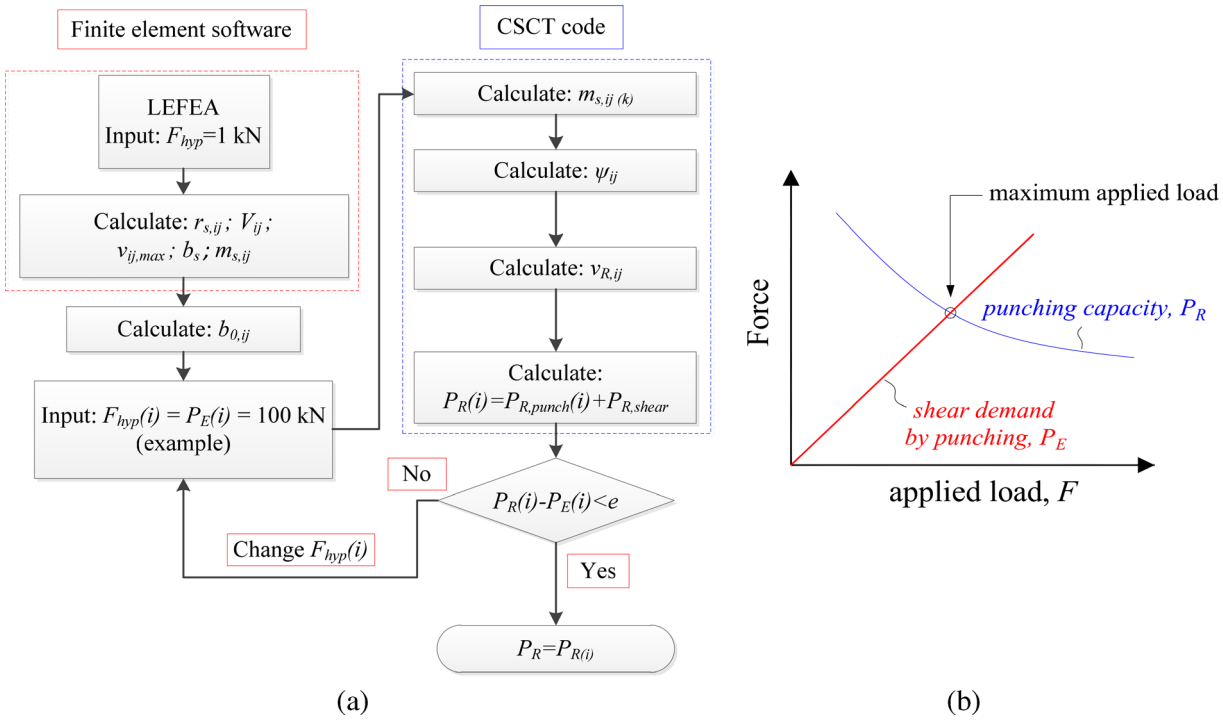

FIGURE 6 (a) Flowchart of the main steps for the evaluation of the punching capacity with the CSCT ($\psi_x - \psi_y$) method; (b) sketch of how the punching capacity is determined in the iterative process. Adapted from.[26]

corners as in Natário,[10] was given by the ratio between the maximum applied unitary shear force perpendicular to the control perimeter ($v_{x1,max}$, $v_{x2,max}$, $v_{y1,max}$ and $v_{y2,max}$) and the total shear force going through that perimeter (V_{x1}, V_{x2}, V_{y1}, V_{y2}) (Figure 5b):

$$b_{0,ij} = \frac{V_{ij}}{v_{ij,max}} \tag{13}$$

Figure 6 shows the main steps to predict the punching shear capacity of slabs coupling LEFEA with the CSCT expressions for non-axis-symmetrical punching shear.[28] First, a LEFEA is carried out to compute the distribution of shear forces ($v_{ij,max} = v_{x1,max}$, $v_{x2,max}$, $v_{y1,max}$, $v_{y2,max}$) and averaged bending moments ($m_{s,ij} = m_{x1}$, m_{x2}, m_{y1}, m_{y2}) over the control sections for an applied load equals 1 kN. At this step, the total shear force on each portion of the control perimeter ($V_{ij} = V_{x1}$, V_{x2}, V_{y1}, V_{y2}) and the flexural strip width b_s shall also be calculated. Afterwards, the reduced control perimeter segments $b_{0,ij}$ are computed for each side of the control perimeter. These values are entered as input in a subroutine that calculates iteratively the punching load $P_E(i)$ that is equal to the punching resistance $P_R(i)$. Notably, the number of outputs of the LEFEA is higher than that required for one-way shear since we need to evaluate the contribution of each control perimeter segment.

A factor was derived by linear regression analyses to avoid overly unsafe predictions of punching capacity for the tests that failed as WBs in one-way shear. Due to the shear flow characteristics of one-way slabs, a smaller portion of the load is transferred by the lateral sides of the control perimeter when the slab width is small (see Figure 7). Therefore, these sides of the control perimeter may have a small contribution to the punching capacity for small values of b_{slab}/l_{load}. Similarly, Setiawan et al.[30,31] also observed that the contribution from some sides of the control perimeter may have a one-way shear behavior, depending on the size of elongated loads or corner walls.

The influence of the ratio slab width-to-load size on the effective contribution of the sides of the control perimeter to the punching capacity (see Figure 7) was not considered by Natário[10] and is considered herein by multiplying the punching resistance $V_{R,y1}$ and $V_{R,y2}$ by a factor β_{width}. This factor was derived assuming that the factor should vary between 0 and 1 and that the contribution of the lateral sides of the control perimeter increases by a square polynomial function. The constants of the polynomial function were adjusted to improve the predictions of punching capacity for a larger dataset of one-way slabs under concentrated loads presented by de Sousa et al.[3]

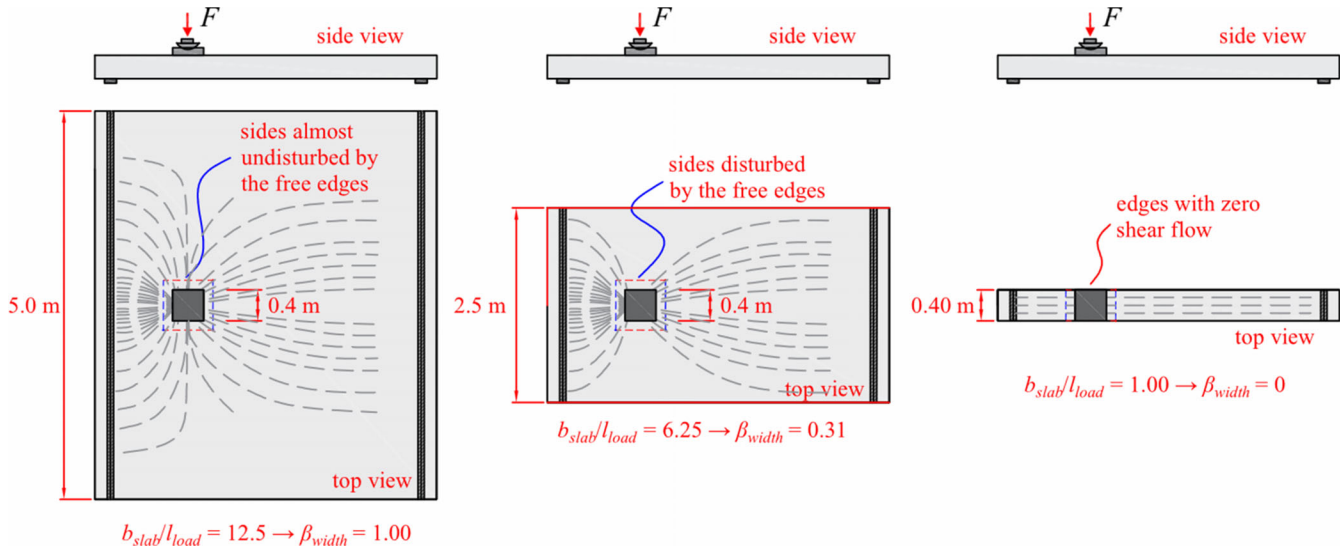

FIGURE 7 Influence of the ratio b_{slab}/l_{load} on the shear flow crossing the sides of the control perimeter parallel to the free edges. Adapted from.[26]

For loads close to simple support:

$$\beta_{width} = \begin{cases} 1 & \text{for } b_{slab}/l_{load} > 7.5 \\ 0.0002 \cdot (b_{slab}/l_{load})^4 \begin{cases} \geq 0 \\ \leq 1 \end{cases} & \text{for } 1 \leq b_{slab}/l_{load} \leq 7.5 \end{cases} \tag{14}$$

For loads close to cantilever supports or continuous supports:

$$\beta_{width} = \begin{cases} 1 & \text{for } b_{slab}/l_{load} \geq 10 \\ 0 & \text{for } b_{slab}/l_{load} < 10 \end{cases} \tag{15}$$

As a result, the following calculations are used to compute the contribution of each side of the control perimeter into the punching capacity (SI units: f_c in MPa; d_g in mm):

$$V_{R,x1} = \frac{1}{\beta_{shear}} \cdot \frac{(3/4) \cdot d_v \cdot \sqrt{f_c}}{1 + 15 \cdot \left[\psi_{x1} \cdot d_v / (d_g + d_{g0})\right]} \cdot b_{0,x1} \tag{16}$$

$$V_{R,x2} = \frac{(3/4) \cdot d_v \cdot \sqrt{f_c}}{1 + 15 \cdot \left[\psi_{x2} \cdot d_v / (d_g + d_{g0})\right]} \cdot b_{0,x2} \tag{17}$$

$$V_{R,y1} = \frac{(3/4) \cdot d_v \cdot \sqrt{f_c}}{1 + 15 \cdot \left[\psi_{y1} \cdot d_v / (d_g + d_{g0})\right]} \cdot b_{0,y1} \cdot \beta_{width} \tag{18}$$

$$V_{R,y2} = \frac{(3/4) \cdot d_v \cdot \sqrt{f_c}}{1 + 15 \cdot \left[\psi_{y2} \cdot d_v / (d_g + d_{g0})\right]} \cdot b_{0,y2} \cdot \beta_{width} \tag{19}$$

The punching capacity for square loads or loads with limited rectangularity ($l_{load} < 3d_v$ and $b_{load} < 3d_v$) is then given by the sum of the capacities of the perimeter segments:

$$P_{R,punch} = V_{R,x1} + V_{R,x2} + V_{R,y1} + V_{R,y2} \tag{20}$$

Slabs subjected to elongated loads exhibit specific characteristics that must be considered. The shear flow assumes a radial pattern in the corners, with a high concentration of shear flow in these regions. Conversely, the shear flow at the elongated sides has lines almost parallel to each other, with a lower demand in this region (Figure 8a). Following the approach proposed by Natário[10] and inspired by the works of Sagaseta et al.,[28] the contribution of the control perimeter in the corners is calculated by the two-way shear expressions ($P_{R,punch}$). In Natário's approach, the same expressions to calculate the one-way shear capacity of such slabs were used in the region with one-way shear behavior, which increased the post-processing effort of the numerical models.

In this study, a simplification was performed on this part of the calculations based on the work from Setiawan et al.[31]

In the proposed modification, when the loaded area is elongated on one of the sides ($l_{load} > 3d_v$ or $b_{load} > 3d_v$), the contribution of the elongated sides not included in the computation of $b_{0,x1}$, $b_{0,x2}$, $b_{0,y1}$ and $b_{0,y2}$ shall be considered with a one-way shear behavior for these lengths (blue lines in Figure 8b). These limits to define the regions with two-way shear behavior and one-way shear

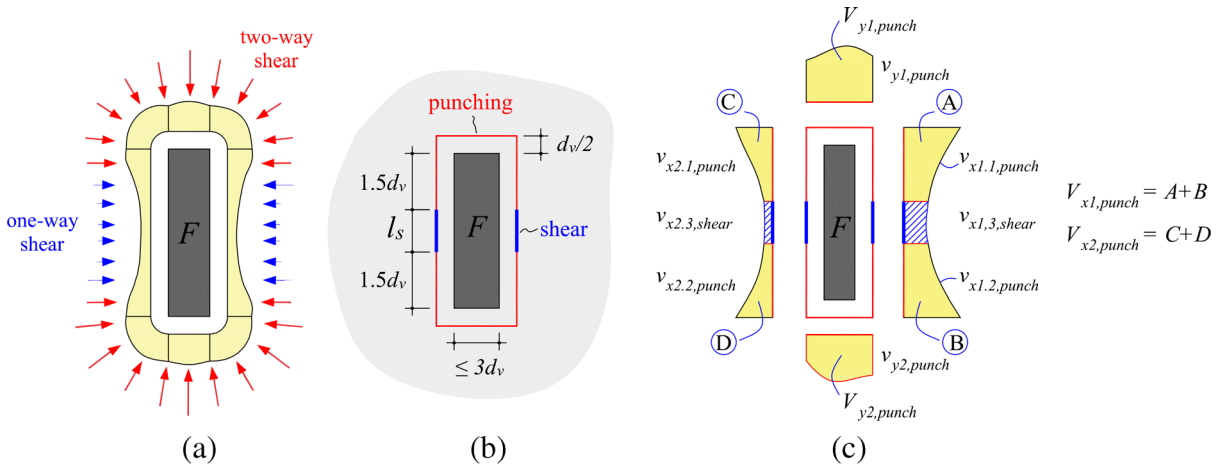

FIGURE 8 (a) Sketch of distribution of nominal shear forces along the control perimeter of elongated loads (assuming only two sides $>3d_v$) with the concentration of shear forces at the corners; (b) lengths of the sides of the control perimeter with two-way shear and one-way shear (control perimeter without rounded corners used in the calculations); (c) sketch of the areas that shall be integrated to determine the shear force distribution around the control perimeter.

behavior are based on the *fib* Model Code 2010.[29] The control perimeter was defined without rounded corners to simplify the post-processing of the numerical models. In practice, four sides of the load can be higher than $3d_v$ and the shape of the load can be square, but the idea remains similar to that applied for elongated loads.

In this study, the contribution of the sides l_s (Figure 8b) is computed according to Setiawan et al.[31] and Cavagnis et al.[32] (assuming only two sides of the load are larger than $3d_v$):

$$P_{R,shear} = v_{c,\min} \cdot (2 \cdot l_s) = \frac{k \cdot d_v \cdot \sqrt{f_c}}{\sqrt{\varepsilon_y \cdot \frac{d_v}{d_{dg}}}} \cdot (2 \cdot l_s) \quad (21)$$

Herein, $v_{c,\min}$ is the minimum shear resistance per unit length (assuming reinforcement yielding), $k = 0.019$, ε_y is the flexural reinforcement yield strain (assumed equal 0.0025 when the material properties of steel were not provided), l_s is the length of the sides assumed with one-way shear behavior (Figure 8), and d_{dg} is the parameter that considers the crack roughness, which is calculated as follows: (SI units: f_c in MPa; d_g in mm):

$$d_{dg} = \min(40\,\text{mm}, 16 + d_g) \text{ for } f_c \leq 60MPa$$
$$d_{dg} = \min\left(40\,\text{mm}, 16 + d_g \cdot \left(\frac{60}{f_c}\right)^2\right) \text{ for } f_c > 60MPa \quad (22)$$

The total punching capacity for elongated loads is given by:

$$P_{predicted} = P_{R,punching} + P_{R,shear} \quad (23)$$

2.3 | Predicting the governing failure mechanism

In a design or assessment task, the most critical failure mode is determined by comparing the concentrated loads F_{Ed} related to the one-way shear failure (V_{Rd}) and the concentrated loads associated with the punching shear failure (P_{Rd}). Therefore, if $F_{Ed,shear} < F_{Ed,punching}$, the one-way shear failure mechanism is theoretically most critical. Consequently, the most critical failure mechanism is defined by the lower ratio between V_{Rd}/V_{Ed} and P_{Rd}/P_{Ed}. At this point, V_{Rd} and V_{Ed} are the design shear actions and shear capacities, respectively. P_{Ed} and P_{Rd} are the respective design punching loads and punching capacities.

Knowing the tested shear V_{test} and punching forces P_{test} from the laboratory tests, and inverting the action and resistance terms, the governing failure mode is therefore determined by the maximum ratio between $P_{test}/P_{predicted}$ and $V_{test}/V_{predicted}$. Herein, P_{test} and $P_{predicted}$ are the tested and calculated punching capacities, respectively; V_{test} and $V_{predicted}$ are the tested and calculated one-way shear capacities. In other words, if the ratio $V_{test}/V_{predicted}$ is higher than $P_{test}/P_{predicted}$, one-way shear is theoretically more critical than punching shear and the predicted governing failure mode would be one-way shear.

In this study, we also calculated the strength ratio (SR) = max $\{V_{test}/V_{predicted}; P_{test}/P_{predicted}\}$ to investigate the global level of accuracy and safety combining the

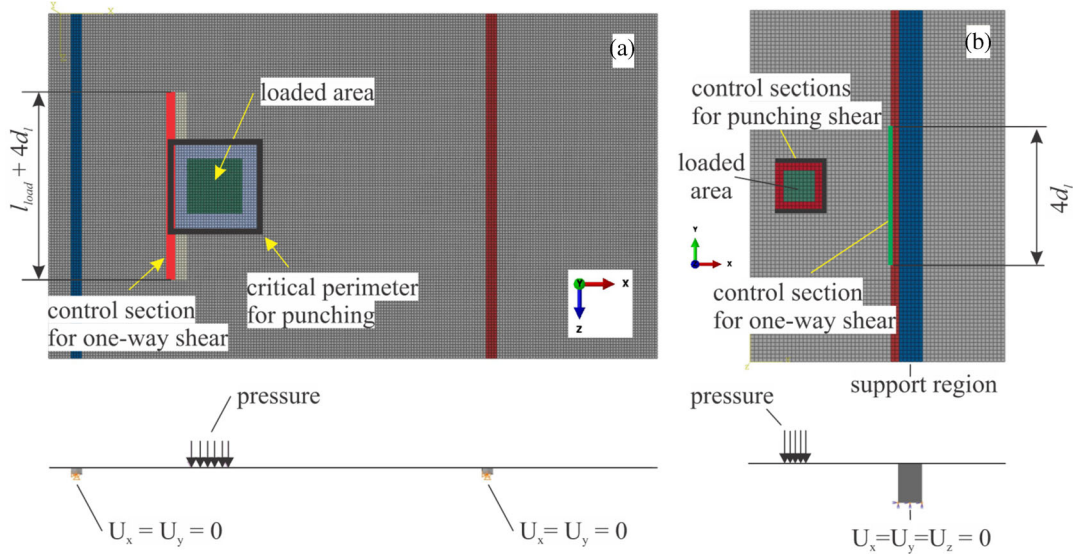

FIGURE 9 Overview of the numerical models developed, highlighting the evaluated regions for one-way shear and punching shear analyses: (a) simply supported test from Reißen et al.[11] and (b) cantilever slab tested from Henze et al.[5]

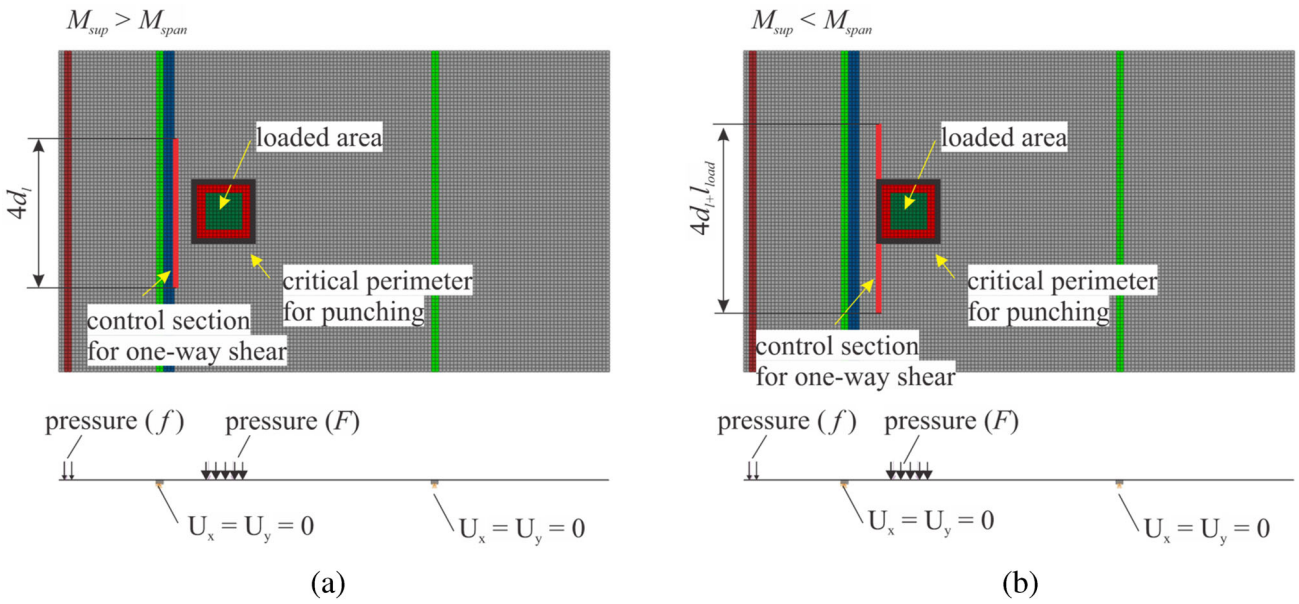

FIGURE 10 Overview of the numerical models developed highlighting the evaluated regions for one-way shear and punching shear analyses: (a) continuous slabs with $M_{sup} > M_{span}$ and (b) continuous slabs with $M_{sup} < M_{span}$.

one-way shear and punching shear predictions. At this point, one can conclude that if the ratios $V_{test}/V_{predicted}$ <1 and $P_{test}/P_{predicted}$ >1, the one-way shear expressions yield an unsafe prediction, but the predicted punching capacity becomes governing.

2.4 | Finite element models

In this study, the finite element software ABAQUS© is used to evaluate the distribution of bending moments and shear forces at the control sections for one-way and two-way shear analyses (Figures 9 and 10). A four-node shell finite element with reduced integration (S4R), hourglass control and finite membrane strains is used to simulate the slab. An eight-node linear brick element with reduced integration and hourglass control (C3D8R) was used to simulate the plate support, and an interface that allows free uplift between the solid supports and the shell elements was applied. Alternatively, compression-only supports could be used along the support axis from the slab, rather than including solid elements with

interaction properties between the shell and the solid elements, as proposed by Natário.[10] In this case, the solid plates would not be necessary in the simulations.

Interface properties of (i) hard contact (free to uplift) and (ii) frictionless are assumed at the contact between the solid plate support and the slab surface for simply supported and continuous slabs. Note that, as the friction coefficient was assumed to equal zero, the normal forces that arise restricting the horizontal displacements at both supports are negligible. Cantilever slabs were simulated rigidly coupled to beam supports. Alternatively, the beam support for cantilever slabs could be removed, and the boundary conditions could be applied directly to the slabs.

The mesh sizes varied in the simulations according to the load size, as suggested in other publications.[33] In practice, we tried to ensure at least eight elements along the control perimeter edges. The vertical displacements are constrained at the support axis on the bottom face of the solid elements, simulating simple supports. The load is simulated by applying uniform pressure with a resulting load equal to 1 kN on the loading area. For continuous slabs (Figure 10), the line load f applied at the overhang in the numerical models corresponds to the same fraction f/F used in the tests, where f is the total load applied at the cantilever member of continuous slabs (see Figure 1b).

The shear modulus of concrete G_c is taken as 1/8 of the calculated value and the Poisson's coefficient ν is assumed to equal 0 to account for the concrete cracking.[1,28,34] Therefore, the following material constitutive law was used for the concrete[10]:

$$\begin{bmatrix} \sigma_x \\ \sigma_y \\ \sigma_z \\ \sigma_{xy} \\ \sigma_{yz} \\ \sigma_{yz} \end{bmatrix} = \begin{bmatrix} E & 0 & 0 & 0 & 0 & 0 \\ 0 & E & 0 & 0 & 0 & 0 \\ 0 & 0 & 0 & 0 & 0 & 0 \\ 0 & 0 & 0 & G & 0 & 0 \\ 0 & 0 & 0 & 0 & \frac{G}{1.2} & 0 \\ 0 & 0 & 0 & 0 & 0 & \frac{G}{1.2} \end{bmatrix} \begin{bmatrix} \varepsilon_x \\ \varepsilon_y \\ \varepsilon_z \\ \varepsilon_{xy} \\ \varepsilon_{yz} \\ \varepsilon_{xz} \end{bmatrix} \quad (24)$$

Here, the modified values of Poisson's coefficient and shear modulus G are intended to represent cracking conditions and significantly influence the distribution of internal forces around the control perimeter, thereby affecting the calculated shear capacity. In other words, the Poisson's ratio of 0 is intended to represent an isotropic material that mimics concrete behavior once cracking begins, and a value of shear modulus equal to G/8 is considered to account for the reduction in shear stiffness as flexural cracks develop. Besides, Setiawan et al.[33] noted that G/8 provides a lower-bound stiffness typical of conditions near failure, where significant shear redistribution has already occurred. In reality, the G value degrades gradually as cracking becomes more severe. Therefore, G/8 is only suitable for predicting the ultimate shear capacity, but it will be less accurate for estimating shear stress distribution during service loads, for instance.

3 | UNDERSTANDING THE TRANSITION FROM ONE-WAY SHEAR TO TWO-WAY SHEAR BASED ON LEFEA

3.1 | Overview

This section reviews the test layout and main parameters of specimens from the literature that can be useful in understanding the transition from one-way shear to two-way shear failures. The tests from Reißen et al.[11] simulate one-way slabs simply supported or with continuity over one of the supports, while the tests from Henze et al.[5] simulate cantilever slabs under concentrated loads. LEFEA was conducted to assess the distribution of shear forces and bending moments at critical sections. These analyses were performed following the recommendations from Section 2.4.

3.2 | Slab width to load size ratio b_{slab}/l_{load}

Different shear failure modes can take place depending on parameters such as the slab width to load size ratio b_{slab}/l_{load}.[35] In the set of tests S15B-1, S25B-1 and S35B-1 tested by Reißen[36] from Figure 11a, the main parameter varied was the slab width b_{slab}, which increased from 1.5, 2.5 to 3.5 m. Consequently, the ratio b_{slab}/l_{load} assumed the values of 3.75, 6.25 and 8.75, respectively.

Figure 11b shows that for the smaller slab widths (S15B-1), the critical shear crack develops a horizontal branch crossing the compression chord of the slab. In other words, the inclined branch of the critical shear crack does not directly reach the frontal load edges (test S25B-1, for instance), which is typical of one-way shear failures in WBs. By increasing the slab width and fixing the other parameters, the critical shear crack crosses the slab mid-height (dashed lines) closer to the loading plate. Besides, the inclined branch of the critical shear crack reaches the load edges (tests S25B1- and S35B-1), a common characteristic of punching failures. Consequently, the punching shear cracks are commonly visible at the compression side of the slabs surrounding the load

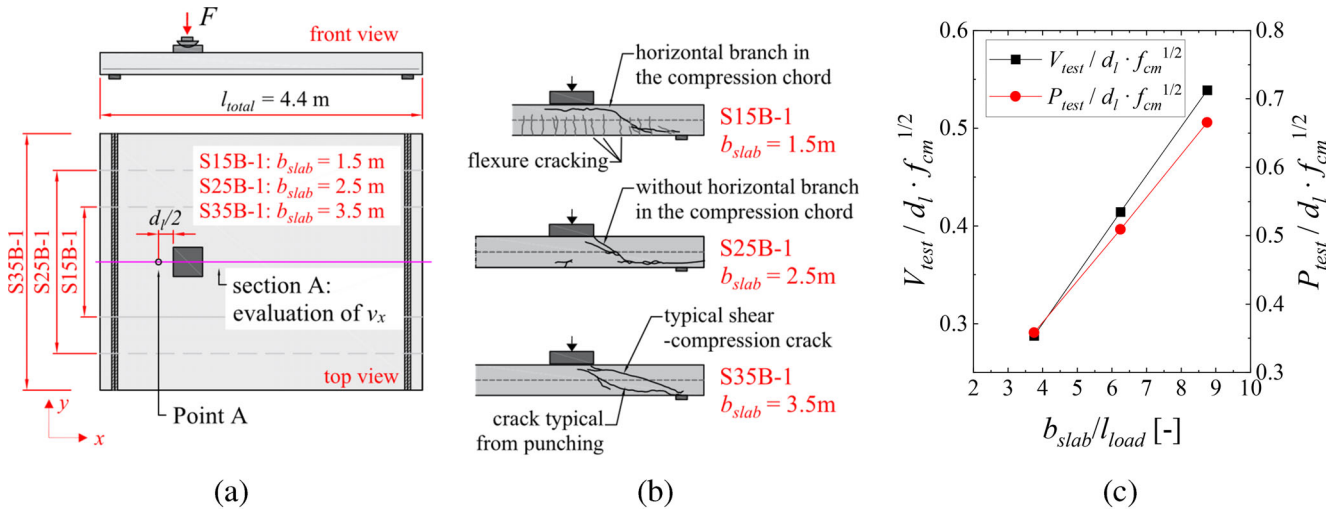

FIGURE 11 (a) Sketch of the tests S15B-1, S25B-1 and S35B-1 from Reißen et al.[11]; (b) Cracking pattern of the same slabs according to b_{slab}; (c) normalized tested shear and punching capacities according to the ratio b_{slab}/l_{load}.

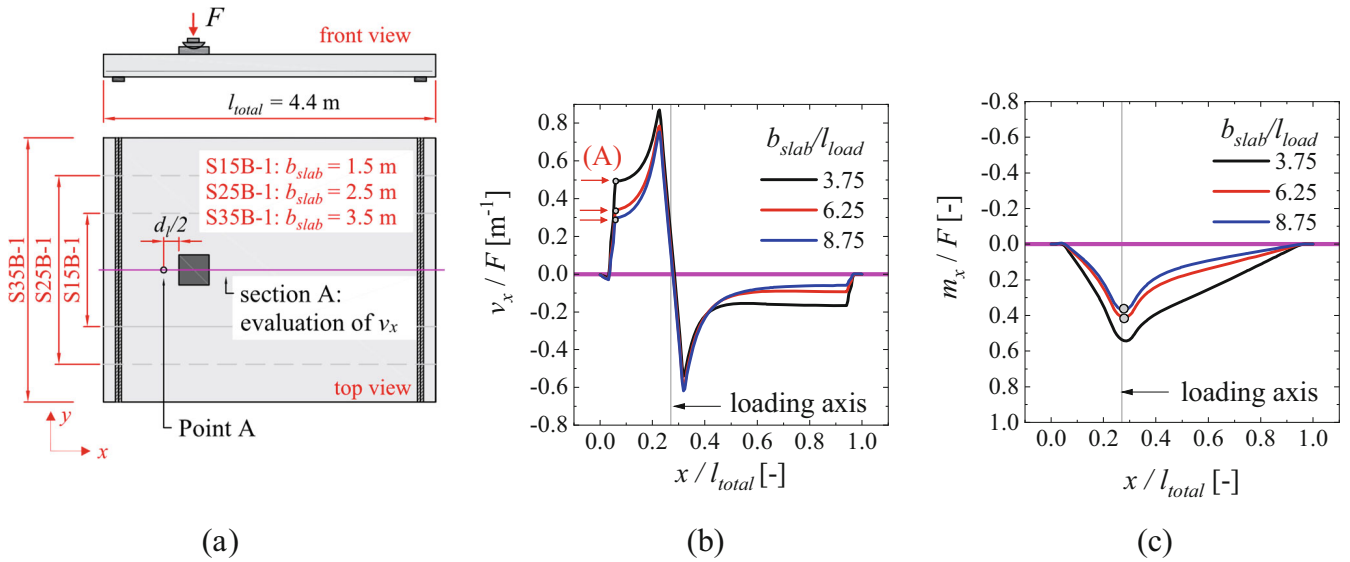

FIGURE 12 (a) Sketch of the tests S15B-1, S25B-1 and S35B-1 from Reißen et al.[11]; (b) distribution of unitary shear forces v_x; and (c) unitary bending moments m_x along the Section A by varying the ratio b_{slab}/l_{load}.

edges.[37] In turn, Figure 11c shows that the tested loads at failure (shear and punching) increased as the ratio b_{slab}/l_{load} increased.

To explain such results in light of the CSCT expressions, Figure 12a shows the effect of increasing b_{slab}/l_{load} on the distribution of shear forces along section A (see Figure 11a) using LEFEA. Increasing the ratio b_{slab}/l_{load} from 3.75 (S15B-1) to 8.75 (S35B-1) decreases the maximum unitary shear force $v_{x,max}$ in the shear span, mainly in the region close to the frontal edge of the load (detail (a) in Figure 12b).

Aided by LEFEA, the elastic effective shear width $b_{eff,el}$ can be calculated as:

$$b_{eff,el} = \frac{V_x}{v_{x,max}} \quad (25)$$

V_x is the sectional shear force assuming a beam model and $v_{x,max}$ is the peak shear force in Point A of Figure 11a. In Figure 12b, one can realize that the $v_{x,max}$ decreases by increasing the ratio b_{slab}/l_{load}. Therefore, the predicted effective shear width according to Equation (24) increases by increasing the ratio b_{slab}/l_{load}. In addition, Figure 12c shows that the bending moments in the x-direction decrease by increasing the ratio b_{slab}/l_{load}. Therefore, an increase in unitary shear capacity in Point A could also be predicted according to the Critical Shear

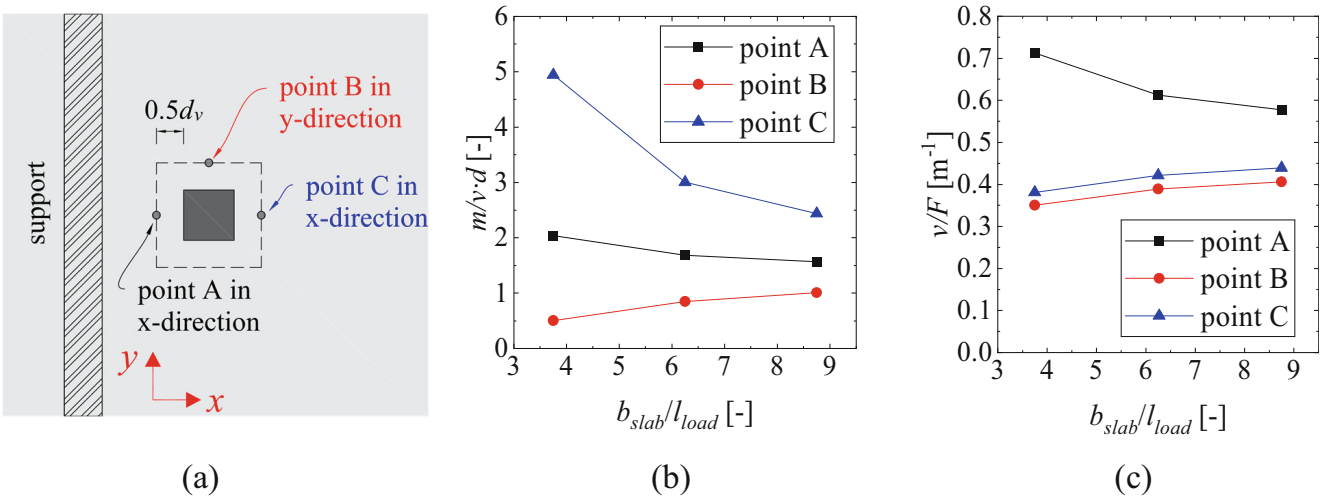

FIGURE 13 (a) Sketch of points A, B, and C evaluated, respectively; the relation between the slab width to load size ratio b_{slab}/l_{load} and (b) the unitary shear force per unit length; (c) the ratio $m/v{\cdot}d$.

Crack Theory.[14] Therefore, the increased shear capacity observed in the tests (Figure 11c) can be well explained according to the CSCT expressions for one-way shear.

To explain the expected behavior in terms of punching capacity, Figure 13 shows the relation between the shear demand v/F and ratio $m/v{\cdot}d$ at points A, B, and C around the load (see Figure 13a), varying the ratio b_{slab}/l_{load}. These points are placed at $d_v/2$ from the load faces in directions x and y, respectively.

Figure 13b shows that as the ratio b_{slab}/l_{load} increases, the shear slenderness $m/v{\cdot}d$ at points A and C (frontal and back sides of the control perimeter) tends to decrease. Consequently, the unitary punching capacity rises consistently in these regions as the slab width increases. Nevertheless, the shear slenderness $m/v{\cdot}d$ at point B (lateral sides of the control perimeter) increases gradually with increasing b_{slab}/l_{load}, which means that the unitary punching capacity on such sides decreases.

Figure 13c also shows that as the slab width increases, the peak shear demand decreases, and the distribution of shear forces around the control perimeter becomes less uneven, which also favors the development of higher punching capacities. However, Figure 13c shows that the ratio m/vd in point B increases considerably by increasing b_{slab}/l_{load} (these numerical results agree with experimental measurements performed by Reißen[36] for the same tests through the instrumentation of the tension reinforcement in the transverse direction). Therefore, the increase in the punching capacity will be a function of the balance between the different resistances and demands over the control perimeter.

Although the shear resistance decreases at point B as the slab width increases, another aspect draws attention. In practice, the predicted shear resistance for these points in slabs with reduced width may be misinterpreted. This occurs because the shear flow concentrates on the frontal and back sides of the control perimeter. Consequently, the contribution of the lateral sides to the punching capacity will be limited. In other words, if the transition between one-way shear and two-way shear is not considered in the problem, the predicted punching capacity for tests with a reduced ratio b_{slab}/l_{load} will be unsafe, as it will be demonstrated in Section 5.1.

3.3 | Influence of the shear slenderness a_v/d_l for simply supported slabs

In the set of tests S35A-1 ($a_v/d_l = 1.9$), S35B-1 ($a_v/d_l = 3.1$) and S35C-1 ($a_v/d_l = 4.4$), the main parameter changed was the shear span a_v and, hence, the shear slenderness a_v/d_l (see sketch of the tests in Figure 14a). In test S35A-1, a shorter span length (3 m) was used compared to other tests, but this parameter was considered secondary for this analysis.

Figure 14b shows that increasing the shear slenderness a_v/d_l from 1.9 to 4.4 changed the governing failure mechanisms from one-way shear (as non-slender WBs) to asymmetrical punching shear. A direct strut between the load and the support was developed when the load was placed closer to the support ($a_v/d_l = 1.9$). The straight shape of the shear crack at failure, without a horizontal branch crossing the compression chord, indicates that arching action occurred at failure. Increasing the shear slenderness to 3.1, a steeper crack develops at the loading edges, together with a flatter crack between the load and the support, indicating a mixed mode between one-way shear and punching. In the test with higher shear

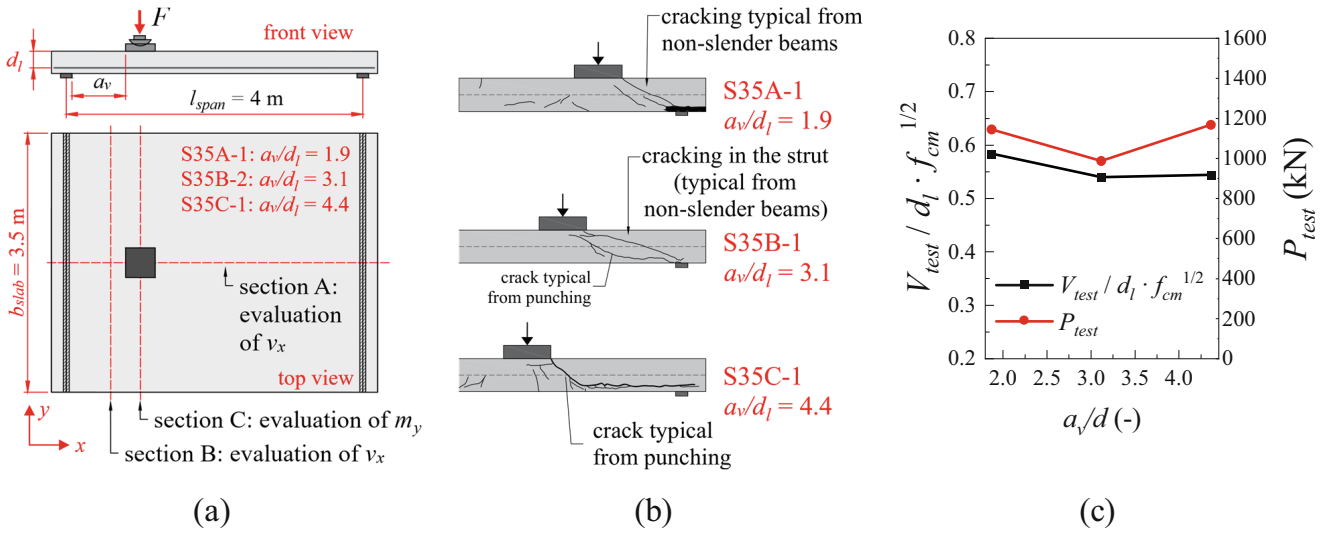

FIGURE 14 (a) Sketch of the tests S35A-1, S35B-1 and S35C-1 from Reißen et al.[11] (*the test S35A-1 was performed with l_{span} = 3 m); (b) Cracking pattern of slabs under concentrated loads close to simple supports from Reißen et al.[11] according to the shear slenderness $\lambda = a_v/d_l$; (c) measured normalized shear force and concentrated load at failure as function of a_v/d_l.

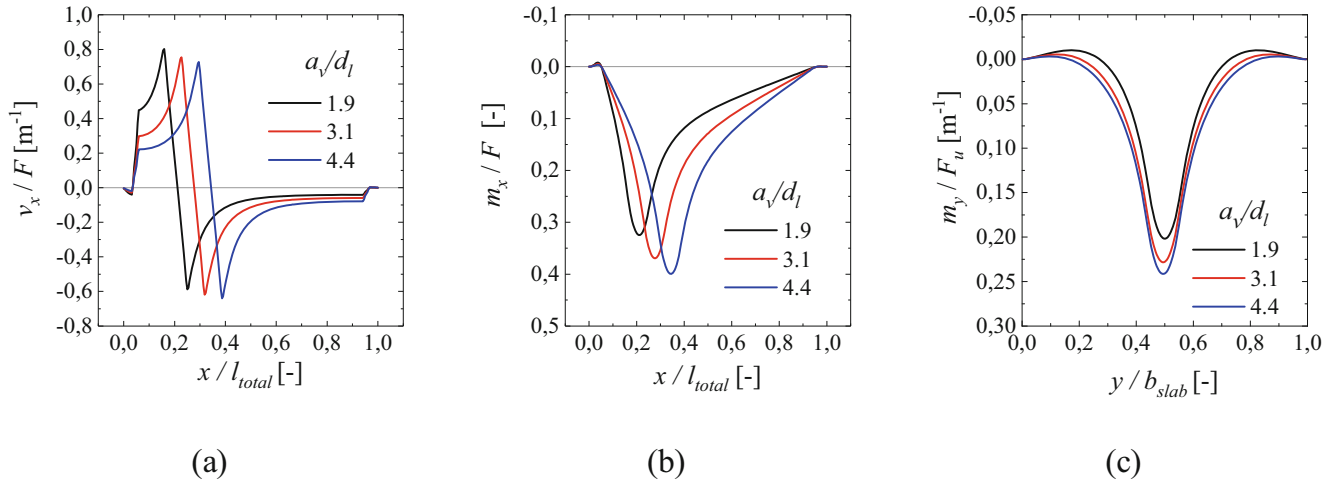

FIGURE 15 Distribution of internal forces of simply supported slabs (sketch in Figure 14) by varying the shear slenderness a_v/d_l: (a) unitary shear forces v_x along the shear span direction (section A); (b) unitary bending moments m_x in along the shear span direction (section A); (c) unitary bending moments my along the transverse direction (section C).

slenderness ($a_v/d_l = 4.4$), the cracking pattern shows asymmetrical punching. Figure 14c shows that the normalized shear force at failure decreased as the shear slenderness increased from 1.9 to 3.1, but kept almost constant when a_v/d_l increased from 3.1 to 4.4. On the other hand, the measured concentrated load at failure P_{test} increased when a_v/d_l varied from 3.1 to 4.4.

In order to explain the test results, Figure 15 shows the effect of increasing the slenderness a_v/d_l in the distribution of shear and bending moments of the slabs. In this example, the following tests from Reißen[36] were evaluated: S35A-1* ($a_v/d_l = 1.9$); S35B-1 ($a_v/d_l = 3.1$) and S35C-1 ($a_v/d_l = 4.4$). In this analysis, the fictitious model S35A-1* was created and used instead of S35A-1, changing the span length from 3 to 4 m to allow a fair comparison with the other tests evaluated (S35B-1 and S35C-1). The test setup was the same as shown in Figure 14a.

Figure 15a shows that the maximum unitary shear forces v_x tend to decrease with increasing shear slenderness a_v/d_l. The ratio V_x/F (being V_x the total shear force going in the direction of the close support), in the same way, also decreases by increasing the shear slenderness. Calculating the elastic effective shear width $b_{eff,el}$ by the ratio $V_x/v_{x,max}$, the $b_{eff,el}$ tends to increase by increasing the shear slenderness (as will be shown in Figure 22b).

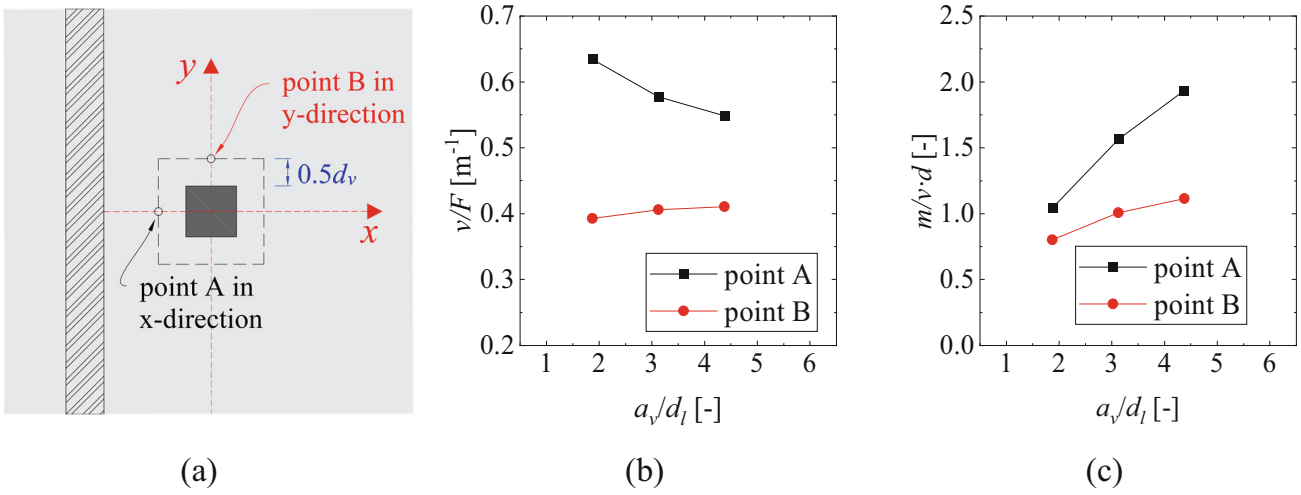

FIGURE 16 (a) Sketch of points A and B evaluated in x and y-directions, respectively; the relation between the shear slenderness with (b) the shear force per unit length at points A and B; (c) the ratio $m/v{\cdot}d$ at points A and B.

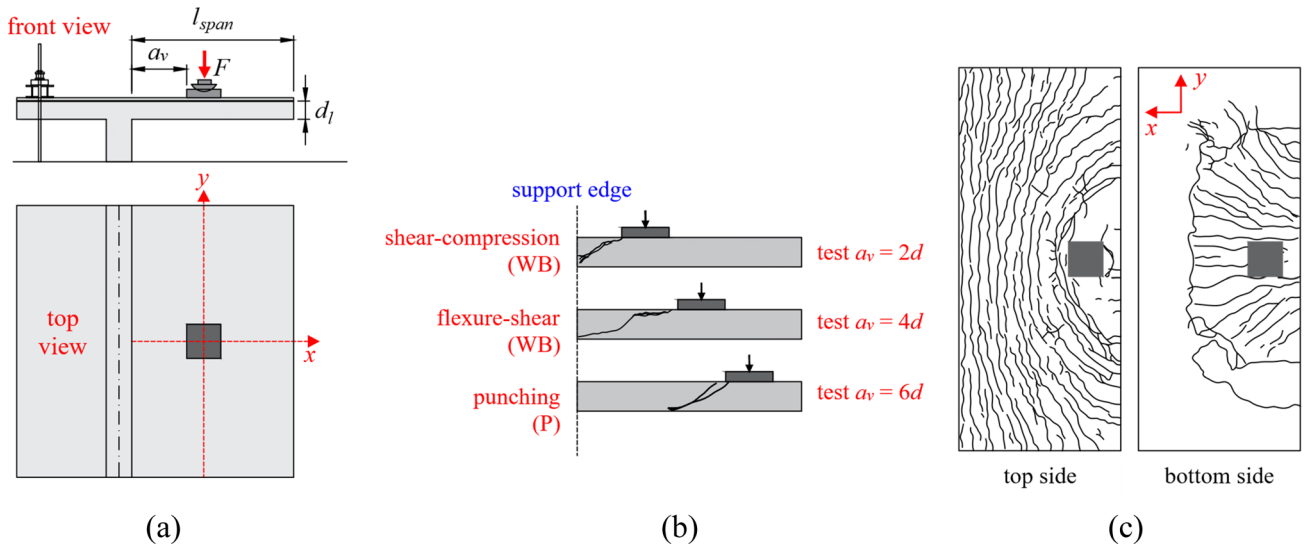

FIGURE 17 (a) Test layout; and (b) cracking pattern in cut view of slabs tested by Henze et al.[5]; and (c) cracking pattern at top and bottom side of test $a_v = 6d$.

At the same time, Figure 15b also shows that the bending moments over the span direction, m_x, increase by increasing the ratio a_v/d_l. Consequently, the unitary shear capacity v_R decreases according to the CSCT Equation (14).

Therefore, the sectional one-way shear resistance V_R (in force units) could increase or decrease depending on combining the effects of the shear slenderness a_v/d_l into the unitary shear resistance and the calculated effective shear width ($V_R = \downarrow v_R \cdot \uparrow b_{\text{eff,el}}$). In practice, the sectional shear load at failure V_R may remain almost the same after the point at which arching action does not influence the resisting mechanisms (see Figure 14c), based on test results from the literature.[1,5,11] Looking at the punching mechanisms, the increase of the bending moments in the x-direction and y-direction (Figure 15b,c) explains the decrease of the unitary punching capacities around the load.

Figure 16 shows how the shear demand and the ratio $m/v{\cdot}d_l$ change at points A and B according to the shear slenderness for simply SSs. When the shear span increases, we observe that the shear demand in point A tends to decrease until a certain plateau, while the shear demand in point B increases to a maximum value. Therefore, increasing the shear slenderness a_v/d_l results in a less uneven distribution of inner forces around the load in such a way that higher punching capacities may be

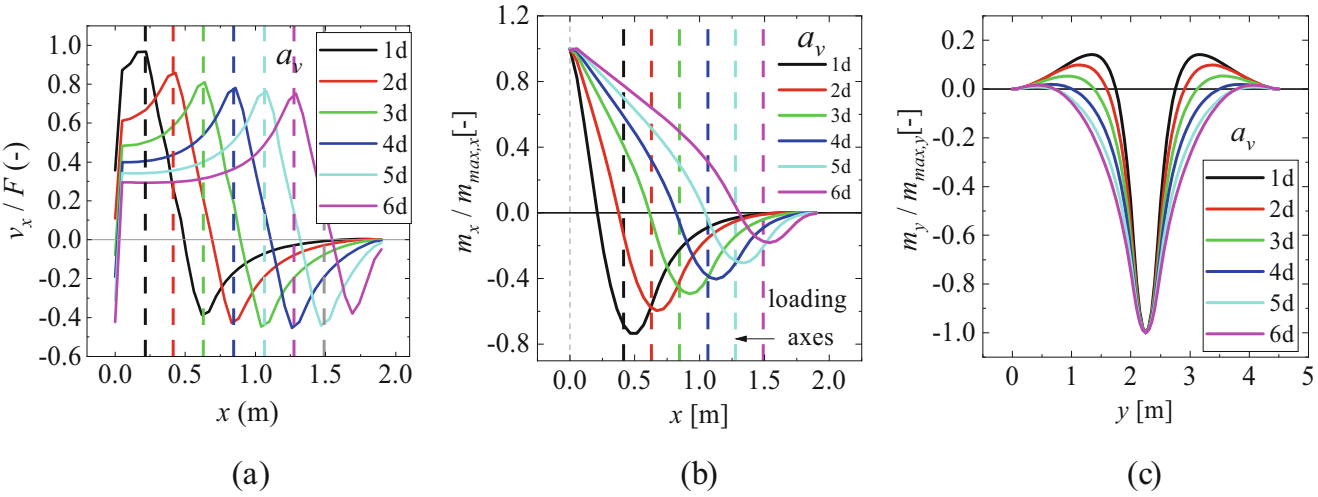

FIGURE 18 Influence of the shear span a_v on the distribution of (a) shear forces over the span direction, (b) bending moments over the span direction, and (c) bending moments over the width direction.

achieved (such as identified in Figure 14c when a_v/d_l increased from 3.1 to 4.4). On the other hand, the ratio $m/v{\cdot}d_l$ tends to increase at both points A and B by increasing the shear slenderness.

In summary, increasing the slenderness has a controversial effect on the one-way shear resistance. While an increase in bending moments reduces one-way shear capacity v_R, a decrease in peak shear forces around the load increases the effective shear width $b_{\text{eff,el}}$. Conversely, the punching resistance seems to be more harmed by increasing the shear slenderness, since the ratio $m/v{\cdot}d_l$ increases at all sides of the control perimeter.

3.4 | Influence of the shear slenderness a_v/d_l for cantilever slabs

Figure 17 shows the cracking pattern for some slabs tested by Henze et al.[5] in cut views. The cracking pattern for loads closer to the support (test $a_v = 1d$) is similar to that of non-slender beams that fail by shear-compression.[38]

The test $a_v = 4d$ from Figure 17b shows a cracking pattern with rebar delamination typical for slender beams failing in flexure-shear. In contrast, the test $a_v = 6d$ presents a cracking pattern typical of punching failures, but without large flexure cracks on the tension side (bottom surface).

Figure 18 investigates the distribution of shear forces and bending moments of the cantilever slabs tested by Henze et al.[5] According to the load position, a_v. Two sections crossing the loaded region are evaluated for each test (Figure 18a). The bending moments measured on the LEFEA, m_x, are normalized by the maximum values $m_{\max}$ of each section (Figure 18b,c).

Figure 18a shows that the peak shear forces in the x-direction decrease as the load distance a_v increases. Consequently, calculating the effective shear width, someone may conclude that the effective shear width $b_{\text{eff,el}}$ would increase as the shear slenderness increases for cantilever slabs.

Different from cantilever beams, slabs develop sagging bending (tension on the bottom) locally around the loaded area (Figure 18b), which may lead to a punching shear failure around the load. Since the bottom reinforcement ratio is usually significantly lower than that placed at the top side, this moment distribution also favors the punching failure of cantilever slabs by cracks arising from the bottom face. However, increasing the distance from the loaded area to the clamped support decreases the amplitude of bending moments across the spanning direction (Figure 18b,c), which means that there is a smoother variation from the peak hogging moment (tension on the slab top side) to the peak of sagging moment (tension on the slab bottom side). Furthermore, the sagging bending close to the loaded area is significantly lower than that at the clamped support for higher shear spans (Figure 18b). Therefore, flexural cracks starting at the bottom face, which could lead to punching failure mechanisms, hardly occur.[10] In test $a_v = 6d$ from Henze,[5] for instance, these flexural cracks were not identified in the shear span direction. However, the sagging moment at the slab width direction (direction y) increases in magnitude as the shear span a_v increases, which is consistent with the cracking pattern observed at the slab bottom side (Figure 17c). Therefore, the bending moments in direction y may trigger a punching failure.

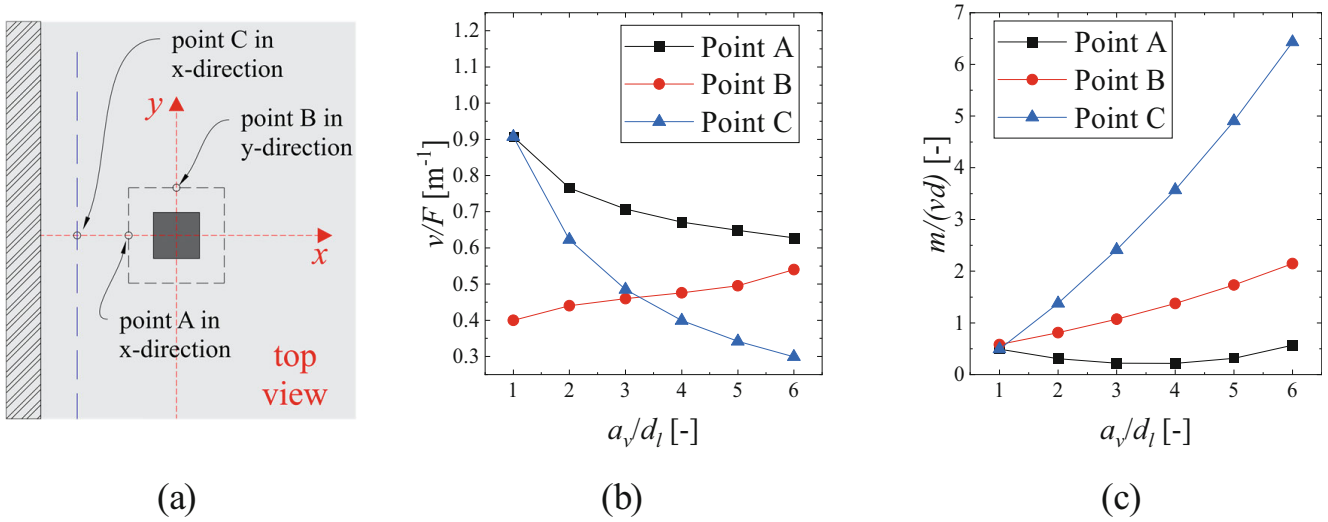

FIGURE 19 (a) Definition of control points A, B, and C used for the evaluation of internal forces; (b) variation of the shear demand per unit length v/F as a function of the shear slenderness a_v/d_l; (c) variation of the bending-to-shear ratio $m/(vd)$ as a function of the shear slenderness a_v/d_l.

Figure 19a shows how the shear forces at the sections far of $d_v/2$ from the load face vary with the shear slenderness a_v/d_l. Points A and B are placed at the control perimeter for punching, while point C is placed at a distance $d_l/2$ from the support edge, which is the usual control section for one-way shear verifications in cantilever slabs.

Figure 19b shows that the shear forces at the front face of the load (point A) decreased as the shear slenderness increased, while the respective shear forces in the transverse direction (point B) decreased. Therefore, the one-way shear failure at the front face of the load becomes less critical as the load distance increases. In literature, it is commonly assumed that as the ratio $m/v{\cdot}d$ increases, the unitary one-way and two-way shear capacities decrease. In this context, Figure 19b shows that the ratio $m/(vd)$ increases substantially in the transverse direction (point B) as the ratio a_v/d_l increases, which decreases the punching capacity in the transverse direction. In the x-direction (point A), the most complex behavior occurs since the ratio $m/(vd)$ decreases until approximately the middle span and increases close to the slab free edge (Figure 19c). Therefore, close to the support and the slab-free edge, the one-way shear and punching shear capacity are depreciated, which is also in line with Setiawan et al.[33] when using advanced finite element analyses.

4 | DATASETS FROM LITERATURE

This study evaluated the one-way shear and punching shear capacity of 112 slabs. This database was published in the public domain,[39] and it includes not only reported information from the references but also input parameters used in the calculations after performing the LEFEA. The test results evaluated were reported by: Damasceno,[40] Ferreira,[41] Ferreira et al.,[42] Regan and Rezai-Jarobi,[43] Reißen,[36] Oliveira,[44] Rombach and Henze,[45] Natário et al.,[1,46] Rombach and Latte,[47,48] Vida et al.[49]

In this dataset, different failure mechanisms were observed: (i) 29 tests failed by punching shear without any reinforcement yielding (P); (ii) 67 tests failed by one-way shear as WBs; (iii) 4 tests presented a mixed failure mechanism between one-way shear and punching shear (WB + P); and (iv) 12 tests were classified as failing by punching after some level of reinforcement yielding (F + P). With respect to the boundary conditions, 60 tests were performed on simply SSs; 7 tests with the load close to the support with slab continuity (CS); and 45 tests with the load applied on a cantilever slab (CT).

Since CSCT expressions were developed to deal only with loads far away from discontinuous regions (a_v/d_l >2.75), tests with lower shear slenderness were kept in the database only if they were performed within an experimental program that included test results with a_v/d_l >2.75 at least. At the end, the dataset evaluated remained with 81 tests with shear slenderness a_v/d_l >2.75 (72.3%) and 31 test results with a_v/d_l <2.75 (27.7%).

Figure 20a shows that most slabs tested have a thickness lower than 0.6 m, and hence do not take into account the size effect important for the assessment of existing solid slab bridges.[50] However, these thicknesses are representative of most reinforced concrete deck girder

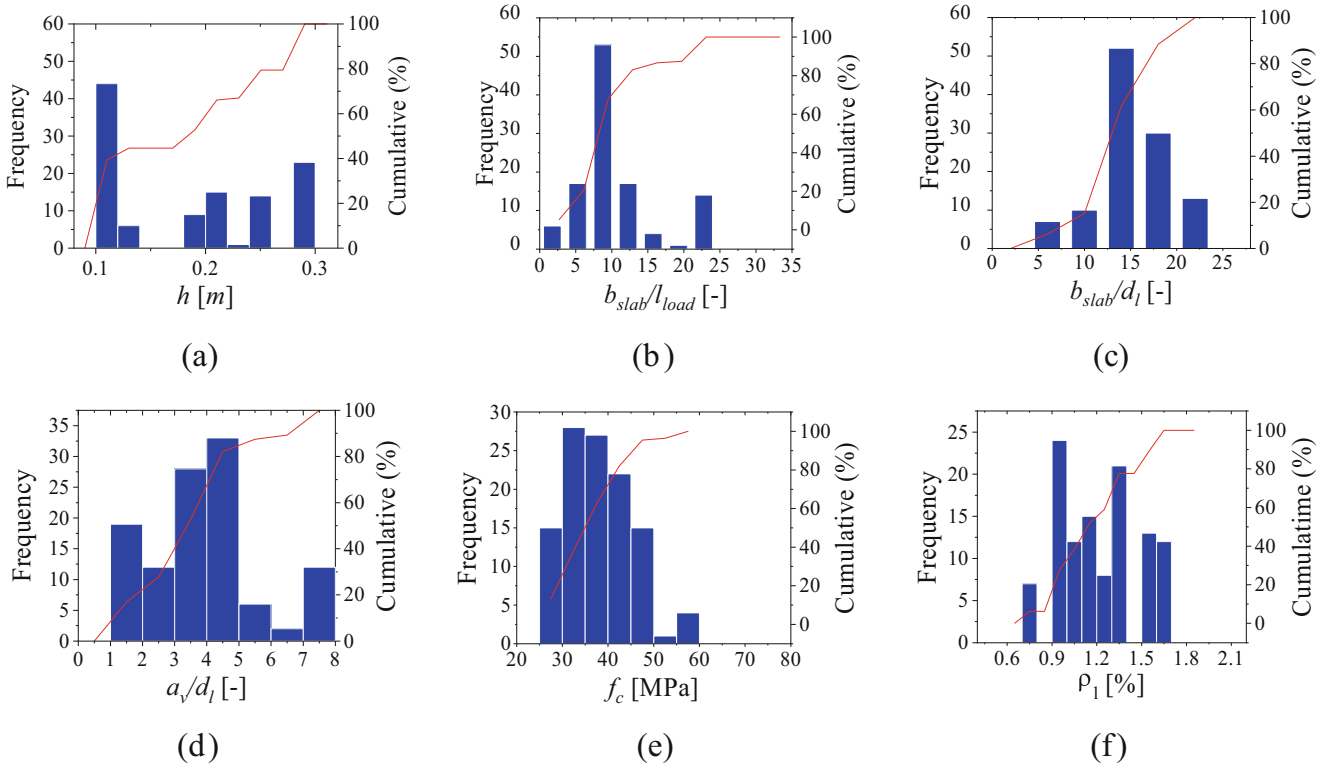

FIGURE 20 Distribution of parameters in the database: (a) slab thickness at the support edge (0.10 m ≤ h ≤ 0.28 m), (b) slab width-to-load size ratio (2.0 ≤ b_{slab}/l_{load} ≤ 21.2), (c) slab width-to-effective depth ratio (4.8 ≤ b_{slab}/d_l ≤ 20.9), (d) shear slenderness a_v/d_l (1.00 ≤ M/Vd ≤7.44); (e) concrete compressive strength (27.9 MPa ≤ f_c ≤ 59.4 MPa) and (f) longitudinal reinforcement ratio (0.71% ≤ ρ_l ≤ 1.69%).

bridges and transversely prestressed concrete decks.[4,51] Figure 20b also shows that more than 85% of the tests were conducted with slab width b_{slab} higher than five times the load size in the width direction l_{load}. This is important because slab strips with very limited width develop a predominantly one-way shear behavior. However, Regan and Rezai-Jarobi[43] also identified punching failures for slabs with ratio b_{slab}/l_{load} equal to 3.33, mainly due to the small slab thickness tested h compared to the effective depth d_l. Figure 20c shows that almost all tests were conducted on specimens with a ratio of b_{slab}/d_l higher than 5 (98%). The only exceptions were tests 1 and 10 from Regan and Rezai-Jarobi.[43] Therefore, most of these specimens are representative for slabs defined according to the German[52] and Brazilian[53] guidelines for reinforced concrete structures.

The shear slenderness a_v/d_l was calculated for all tests to identify which ones could be influenced by arching action. Figure 20d shows that most of the tests (approximately 72%) were conducted with a_v/d_l >2.75 and hence, arching action probably did not influence most of the test results. On the other hand, 28% of the tests may have developed arching action between the load and the support[1,54] and failed as non-slender beams in one-way shear. In these cases, and based on previous studies,[53,54] we applied a β factor to capture the capacity enhancement when the failure mode changes from flexure-shear to shear-compression.

Figure 20e shows that the tests evaluated were conducted with usual concrete compressive strengths (high-strength concretes were not covered in this study). Besides, Figure 20f shows the longitudinal reinforcement ratios in the tests are similar to those used on beam-shear experiments, which means that most tests have ρ_l >1% to assure shear failure mechanisms.

5 | RESULTS

5.1 | Predictions according to the ratio b_{slab}/l_{load}

In order to illustrate the impact of the proposed changes on the predictions of punching capacity, a set of tests on which the slab width and, consequently, the ratio b_{slab}/l_{load} varied from 3.75 to 8.75 (tests S15B-1, S25B-1 and S35B-1 from Reiβen et al.[11]) was evaluated. The tests with b_{slab}/l_{load} equal 3.75 and 6.25 were classified as failing in one-way shear (WB), while the test with b_{slab}/l_{load} = 8.75 failed in a mixed mode between one-way shear and two-

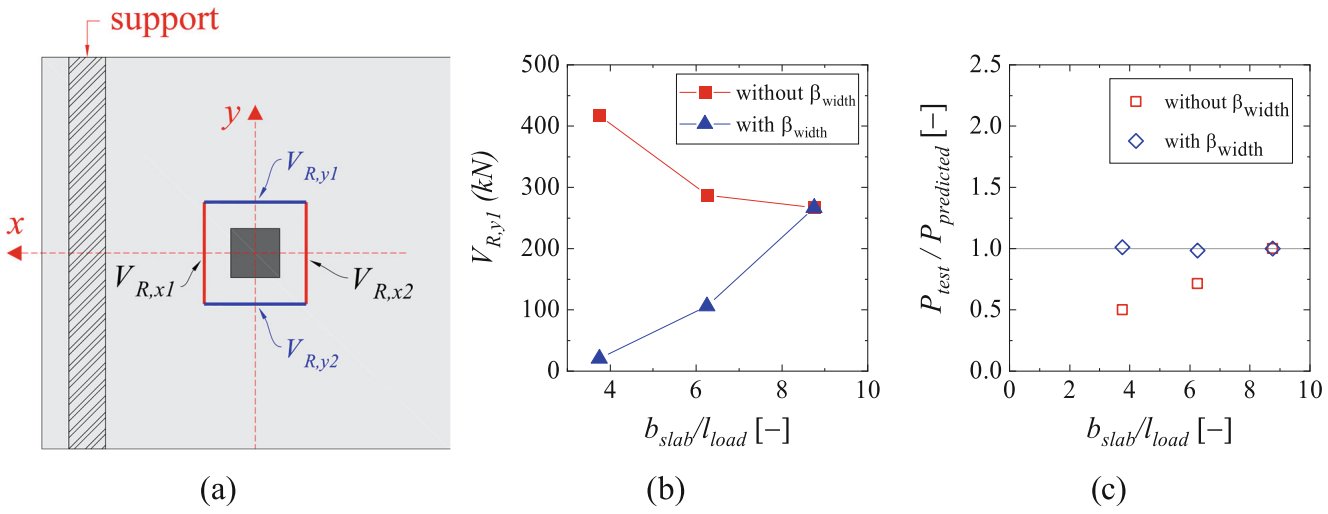

FIGURE 21 Influence of considering or not the correction factor related to the slab width (β_{width}) on the predictions of punching capacity: (a) notation of the sides in the control perimeter; (b) relation between the predicted contribution $V_{R,y}$ with b_{slab}/l_{load}; and (c) influence of the ratio b_{slab}/l_{load} on the ratio between tested and predicted punching capacities.

way shear (WB + P). Figure 21a illustrates the notation used for each side of the control perimeter, depending on the load position. Figure 21b shows that, without considering the proposed correction factor β_{width}, the contribution of the lateral sides of the control perimeter tends to decrease by increasing the ratio b_{slab}/l_{load} due to increased slab rotation ψ expected for this side based on the CSCT principles.[15] Nevertheless, it draws attention that the contribution from these sides ($V_{R,y1} = V_{R,y2}$) to the total punching capacity tends to be overestimated for slabs with reduced slab width and that failed in one-way shear. In other words, as the shear flow tends to concentrate on the frontal and back sides of the control perimeter ($V_{R,x1}$ and $V_{R,x2}$) when decreasing the slab width, the contribution from the lateral sides should decrease as the ratio b_{slab}/l_{load} increases, which is only correctly represented including the proposed correction factor (Figure 21b).

Figure 21c compares the tested and predicted resistances using the punching shear expressions with and without the proposed changes. While the original approach, without the correction factor, tends to yield overly unsafe predictions for tests that failed in one-way shear, the proposed approach allows for improved accuracy in those predictions, even though these tests did not fail by punching. In other words, it can be stated that considering a correction factor related to the transition between one-way shear and two-way shear failure mechanisms in the punching shear verifications allows for improving the predictions when the critical failure mechanism may be the one-way shear.

5.2 | Predictions according to the shear slenderness a_v/d_l

Figure 22 evaluates in detail the influence of the shear slenderness a_v/d_l for the set of test results S35A-1, S35B-1, and S35C-1 from Reißen et al.,[11] on which the a_v/d_l assumed the values of 1.88, 3.13, and 4.38, respectively. Figure 22 shows that, despite the predicted unitary one-way shear capacity tending to decrease with increasing shear slenderness, the predicted effective shear width increases, as explained in Section 3.3, as the peak shear stresses at the control section tend to decrease by increasing a_v/d_l. Therefore, the predicted shear capacity, $V_{R,CSCT}$, may increase or decrease depending on the combination of these parameters, namely $v_{R,shear}$ and b_{eff}.

Nevertheless, Figure 22b shows that the presented approach by Natário et al.[1] to predict the one-way shear capacity allows for representing very well the observed trends in the test results from Reißen et al.,[11] in which the tested one-way shear capacities decreased when the shear slenderness increased from 1.88 to 3.13 and shear capacity decreased when a_v/d_l changed from 3.13 to 4.38. Besides, Figure 22 shows that combining the tested and predicted resistances for one-way shear and two-way shear using the presented approaches allowed for excellent levels of precision for the SR, with an average value of 1.15 and a coefficient of variation equal 16.9%. In addition, comparing the predictions of one-way shear and two-way shear, the governing failure mechanism was correctly predicted in the three tests (one-way shear for $a_v/d_l = 1.88$ and a mixed mode or two-way shear for $a_v/d_l = 3.13$ and 4.38).

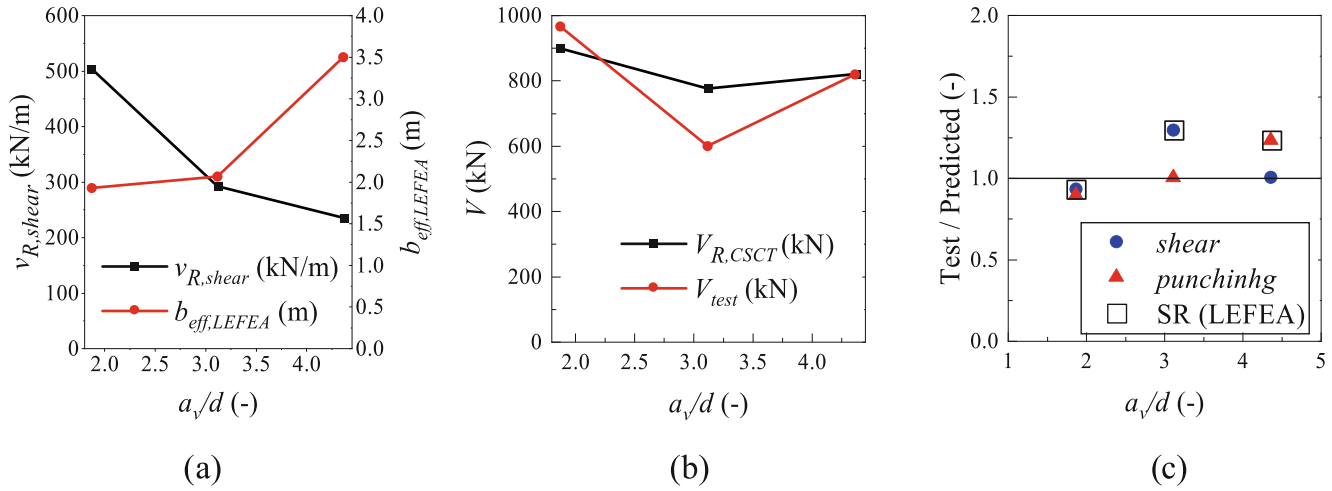

FIGURE 22 Influence of the shear slenderness a_v/d_l on (a) predicted unitary shear capacity $v_{R,CSCT}$ (kN/m) and effective shear width $b_{eff,LEFEA}$ (m); (b) tested and predicted one-way shear capacities according to Section 2.1; and (c) the comparison between tested and predicted resistances using the proposed approach for one-way shear and two-way shear predictions.

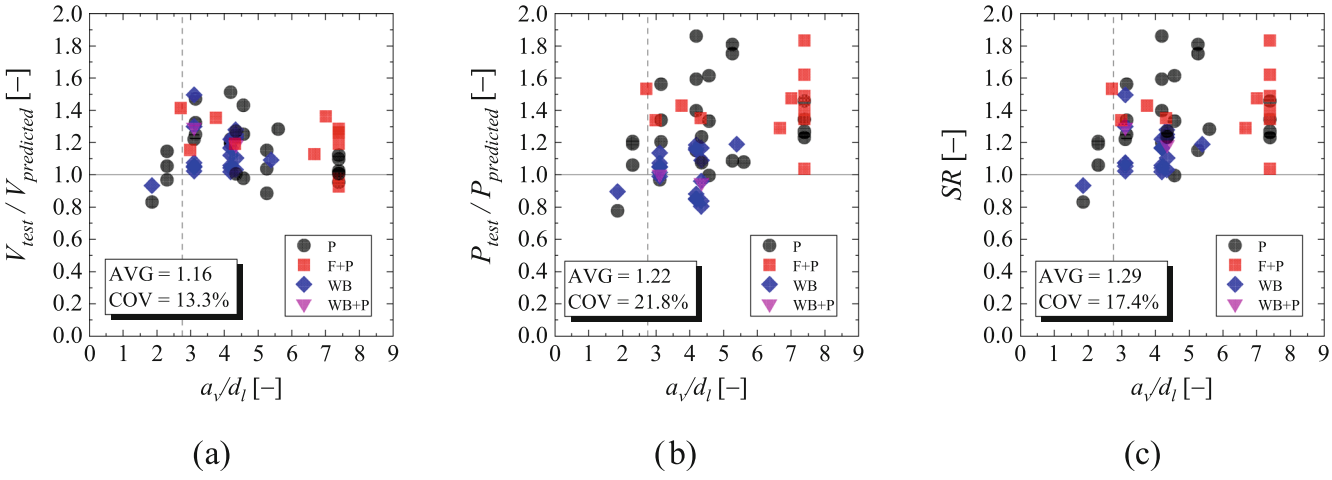

FIGURE 23 Comparison between tested and predicted capacities for simply supported slabs under concentrated loads using (a) one-way shear expressions, (b) two-way shear expressions and (c) maximum shear strength ratio (SR).

5.3 | Simply supported slabs: 60 test results

Figure 23 compares the predictions of one-way shear and punching shear capacities for 60 simply SSs tested under a single concentrated load. The results are plotted according to the governing failure mechanism (reported in references or classified in this study according to previous publications[12]) being one-way shear as WBs, punching shear without reinforcement yielding (P), punching shear after some level of reinforcement yielding (F + P), and a mixed failure mechanism between one-way shear and punching. Figure 23c shows the most conservative SR given by the maximum value between tested and predicted resistances for shear and punching shear predictions (SR = max{$V_{test}/V_{predicted}$;$P_{test}/P_{predicted}$}).

Figure 23a shows that using the one-way shear model based on the CSCT combined with LEFEA allows for accurate and precise predictions of one-way shear capacity regardless of the failure mode from the tests (one-way shear or two-way shear). The average ratio between the tested and predicted one-way shear capacities was 1.16 with a coefficient of variation of 13.3%. Comparatively, Figure 23b shows the punching shear predictions provided a higher scatter between experimental and predicted resistances, with an average ratio of 1.22 and a coefficient of variation of 21.8%. Notably, some predictions of punching capacity still

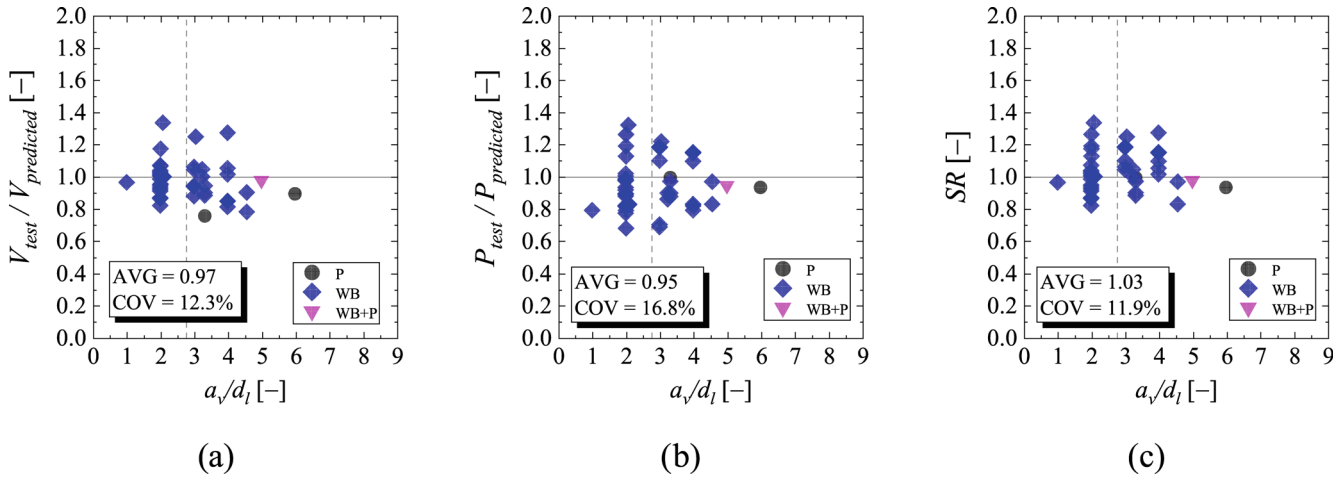

FIGURE 24 Comparison between tested and predicted capacities for cantilever slabs under concentrated loads using (a) one-way shear expressions, (b) two-way shear expressions and (c) maximum shear strength ratio (SR).

resulted on the unsafe side when the test results presented a one-way shear failure mechanism (WB). These predictions occurred mainly for slabs with a reduced ratio between slab width and load size. Using the maximum SR between the one-way and two-way shear resistance predictions, the predicted resistances are always conservative (SR >1). The average ratio between tested and predicted resistances was 1.29 with a coefficient of variation equal 17.4%. Besides, it was observed that this approach predicted the shear mechanism in 81.7% of the cases correctly. When the correct failure mechanism was not predicted, a conservative prediction of the shear or punching shear capacity occurred.

Figure 23 also shows interesting insights regarding the prediction trends. Comparing the predictions between one-way shear and two-way shear expressions, someone may realize that the precision level of the one-way shear approach is less sensitive to the shear slenderness a_v/d_l, while the predictions tend to be more conservative in the two-way shear expressions by increasing the shear slenderness. In practice, this can be fact that the failure is almost always triggered at the frontal side of the load. Besides that, the unitary shear capacity in one-way shear and two-way shear is both deprecated by increasing the shear slenderness. Consequently, the one-way shear approach (LEFEA + CSCT) may provide accurate predictions of ultimate capacity even when punching shear is governing.

5.4 | Cantilever slabs: 45 test results

Most previous studies do not address the punching capacity of cantilever slabs under concentrated loads close to the support, with the argument that the one-way shear capacity tends to be the governing failure mode.[6,10] However, some punching failures were observed in cantilever slabs tested by Henze et al.[5] (Figure 17, test $a_v = 6d$). Figure 24c shows that the combination of CSCT expressions for one-way shear with LEFEA allows for accurate prediction of the one-way shear capacity of the tests. The mean ratio V_{exp}/V_{CSCT} is 0.97 with a coefficient of variation of 12.3%.

These results are consistent with Figure 19b,c, where it was demonstrated that the one-way shear mechanisms tend to govern the shear capacity of cantilever slabs due to the lower ratio m/vd around the load compared to close to the support. However, it was identified that the predictions of one-way shear capacity become slightly unsafe when the governing failure mode changes from one-way shear to two-way shear, increasing the shear slenderness a_v/d_l to values above 4 (Figure 24a). For ratios $0 \leq a_v/d \leq 4$, the average ratio $V_{test}/V_{predicted}$ was 0.98 (COV = 12.3%), while in the range of a_v/d >4, the same average ratio was 0.89 (COV = 9.1%).

Figure 24b shows that the punching shear approach tends to overestimate the capacity for some tests that failed in one-way shear as WBs. Because of this, the average ratio between tested and predicted resistances was 0.95 with a coefficient of variation of 16.8%. However, the predictions for the tests that failed by punching or a mixed mode between one-way shear and punching shear are close to the tested values. For instance, the punching predictions for the load far from the support (test $a_v = 6d$) deviate only 7% from the experimental value, which indicates that the punching model provided closer predictions of the SR for this specimen. Notably, test $a_v = 5d$ showed almost the same SR for one-way and

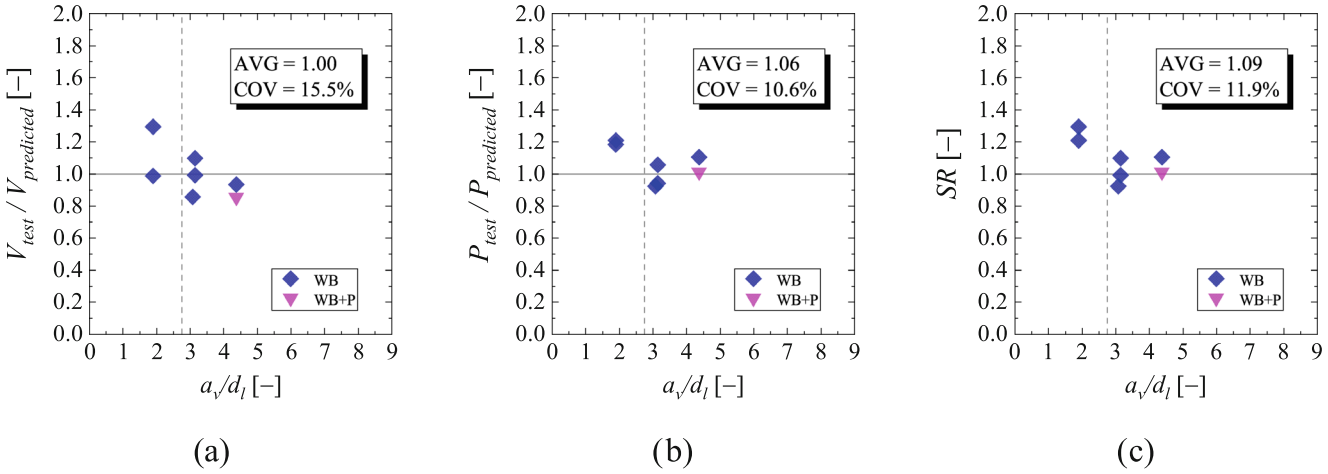

FIGURE 25 Comparison between tested and predicted resistances for continuous slabs under concentrated loads using (a) one-way shear expressions, (b) two-way shear expressions and (c) maximum shear strength ratio (SR).

two-way shear analyses, which indicates that this test could fail by any shear failure mechanism.

Combining the one-way shear and punching shear resistance predictions (Figure 24c), the average ratio SR was 1.03 with a coefficient of variation of only 11.9%. Consequently, combining the shear and punching shear predictions increased only slightly the safety margin compared to using only the one-way shear approach. Regarding the prediction of the governing failure mechanism, the calculations indicated that the critical failure mechanism was correctly predicted in only 74.5% of the tests, which is very similar to the ones achieved for simply SSs.

5.5 | Continuous slabs: 7 test results

Figure 25 compares the tested and predicted resistances for continuous slabs under concentrated loads using one-way shear expressions, punching shear expressions, and a combined prediction. In general, the predictions for one-way shear and punching shear capacity showed similar levels of accuracy for this dataset.

The average ratio between tested and predicted resistances was 1.00 (COV = 15.5%) using the one-way shear expressions and 1.06 (COV = 10.6%) using the punching shear expressions. These results indicate that in the continuous slabs evaluated, the one-way shear and punching shear capacities were very close. In fact, in the tests with larger shear slenderness, some tests started to fail by punching or a mixed mode between one-way shear and two-way shear.

Comparing the predictions of one-way shear and punching shear resistance, the governing failure mechanism was correctly predicted in 4/7 cases (approximately 57.1%). This means that, even under more complex boundary conditions, the combination of the LEFEA + CSCT method allows for predicting well the behavior of continuous slabs under concentrated loads at ultimate limit states.

5.6 | Comparison between the presented approach and approaches from the literature

Table 1 shows the comparison between the tested and predicted resistance using the presented approach, combining LEFEA + CSCT expressions (Section 2), and also using the expressions from the current EN 1992-1-1:2023[55] with recommendations from Halvonik et al.[6] regarding the definition of the effective shear width (more details in Appendix A).

Table 1 shows that the presented approach (LEFEA + CSCT) achieves higher accuracy than current approaches that use only analytical expressions, regardless of the boundary conditions. In general, the average ratio between tested and predicted resistances with the LEFEA+CSCT method varies between 0.97 and 1.16, with COVs <15% using the one-way shear expressions. On the other hand, when using European code expressions, the average ratio $V_{test,red}/V_{predicted}$ varies between 1.06 and 1.36.

Using the punching shear expressions, the LEFEA + CSCT methods also stand out compared to the fully analytical approach. The average ratio $P_{test}/P_{predicted}$ varied between 0.95 and 1.22 according to the support conditions in the LEFEA + CSCT method, while the same ratio varied between 0.97 and 1.30 in the fully analytical method.

In other words, the fully analytical approach yields slightly more conservative predictions for most of the tests. Nevertheless, it shall be highlighted that such

TABLE 1 Comparison between tested and predicted resistances using the one-way shear expressions, punching shear expressions, and combining both predictions (SR) for the presented approach (LEFEA + CSCT) and the Eurocode 2 expressions.[55]

Support condition	Statistics parameter	$\frac{V_{test}}{V_{predicted}}$	$\frac{P_{test}}{P_{predicted}}$	SR [−]	$\frac{V_{test,red}}{V_{predicted}}$	$\frac{P_{test}}{P_{predicted}}$	SR [−]
		LEFEA + CSCT	LEFEA + CSCT	LEFEA + CSCT	Eurocode + Appendix A	Eurocode + Appendix A	Eurocode + Appendix A
CT (45)	AVG	0.97	0.95	1.03	1.06	1.30	1.31
	MIN	0.75	0.67	0.82	0.83	0.94	1.01
	COV	12.3%	16.8%	11.9%	14.8%	16.8%	16.1%
CS (7)	AVG	1.00	1.06	1.09	1.36	0.97	1.36
	MIN	0.85	0.92	0.92	1.16	0.79	1.16
	COV	15.5%	10.6%	11.9%	12.1%	11.9%	12.1%
SS (60)	AVG	1.16	1.22	1.29	1.06	1.15	1.22
	MIN	0.83	0.77	0.83	0.76	0.61	0.83
	COV	13.3%	21.8%	17.4%	19.3%	20.8%	18.5%
All (112)	AVG	1.07	1.10	1.17	1.08	1.20	1.27
	MIN	0.75	0.67	0.82	0.76	0.61	0.83
	COV	15.6%	23.3%	18.9%	18.2%	20.2%	17.4%

analytical results excel compared to previous publications on this field that applied the replaced Eurocode expressions combined with other effective shear width expressions[56] (on which the effective shear width would increase indefinitely as the shear span increases). Therefore, it can be stated that the use of the current EN 1992-1-1:2023 combined with the proposed effective shear width by Halvonik et al.[6] may also provide good predictions of one-way shear capacity, mainly for a preliminary analysis of large bridge stocks.

6 | DISCUSSION

Most studies related to one-way slabs under concentrated loads close to the support focused on the assessment by the combination of one-way shear models with an effective shear width.[1,5,6,11] However, these slabs may also fail by punching or a transitional failure mode between one-way shear and two-way shear.[2,12,13] Because of this, the coupling of one-way shear models and two-way shear models is essential to predict the governing failure mode[10] and reach enhanced levels of safety in design and assessment. In this study, we observed that, combining the one-way shear and punching shear expressions with LEFEA, the correct failure mechanism would be approximately 81.7% for simply SSs, 74.5% for cantilever slabs, and 57.1% for continuous slabs. For continuous slabs, the lower predicted rate could be attributed to the complex load distribution under these support conditions, which hampers distinguishing one-way shear from two-way shear.[12,33] Considering the entire database of 112 test results, the correct failure mechanism was predicted in 86 of 112 tests, for a 76.8% success rate. Nevertheless, it should be noted that, when the correct failure mechanism was not identified, at least conservative predictions of capacity occurred.

In the studies that used semi-empirical punching shear expressions to predict the punching capacity of slabs under concentrated loads, a higher dispersion between predicted and experimental results was found[13,56] because the punching capacity is overestimated for slabs that fail as WBs. Herein, this limitation was partially mitigated in the proposed approach, LEFEA + CSCT, by applying the correction factor β_{width}, based on the slab width-to-load size ratio (b_{slab}/l_{load}), which improved predictions of ultimate capacity even when tests failed due to one-way shear.

Comparing the predictions of one-way shear and punching shear capacities, we can also realize that the one-way shear capacity predictions frequently led to enhanced levels of accuracy, even when the tests failed by punching, and regardless of the support conditions (Figures 23–25). In fact, the failure mechanism of one-way slabs under concentrated loads almost always takes place locally around the concentrated load on the most heavily loaded side, regardless of whether the test fails by one-way shear or punching. Therefore, it is fair to say that the predicted one-way shear capacity matches the tested resistance well in most cases when using the one-way shear expressions. At the same time, this also explains why it is more difficult to reach the same level

of accuracy with the punching shear expressions. As the punching shear expressions assume that the whole control perimeter contributes to the punching capacity, this approach tends to overestimate the test resistance when the slab fails only locally around the load and on one of the sides for one-way shear. When the tests fail by punching, on the other hand, the failure mechanism frequently develops along a larger portion of the control perimeter, even in asymmetrical punching.

Until now, the assessment of the punching shear capacity of cantilever slabs has not been frequently discussed[34] and most publications addressed this problem using only semi-empirical code expressions.[34] In this study, it is shown that CSCT expressions can accurately predict the resistance of cantilever slabs when they are critical in punching, as observed in the test results of Henze et al.[5] when the shear slenderness increased to $a_v/d_l \geq 5$. Besides that, it was shown that, by comparing the predictions of one-way shear and punching shear for cantilever slabs, it was possible to predict the governing failure mode of most test results at different locations from the support. However, it was also shown that the occurrence of punching failures on cantilever slabs is complex since the bending moments that develop close to the loaded area are significantly lower than those at the support.

It should be noted that, compared to approaches using non-linear finite element analyses (NLFEA), LEA-FEA requires a much lower number of input parameters for the numerical models. Besides that, the numerical model processing is faster when using shell elements than when using three-dimensional models to simulate the slab. In this study, the average ratio between tested and predicted resistances for the whole database, covering 112 test results, was 1.07 (COV = 15.6%) for one-way shear and 1.10 (COV = 23.3%) for punching shear. In a previous publication from our group,[57] the NLFEA was applied to 13 test results related only to simply SSs, and the ratio between tested and predicted resistances, in terms of the concentrated load, reached an average ratio of 1.07 (COV = 11%). Therefore, the presented approach, grounded in simplified finite element analyses and a sound theory to predict shear capacity, achieved an accuracy comparable to that of calibrated NLFEA, even when applied to a significantly bigger database.

In the case of fully analytical predictions, this study also presents new insights. The first one is the use of the one-way shear expressions from EN 1992-1-1:2023[55] combined with the proposed effective shear width by Halvonik et al.[6] may also provide excellent levels of accuracy compared to previous publications in this field. In practice, this may be attributed to the improved expressions for shear capacity in the new code and to the enhanced effective shear width model. Besides that, the use of the updated expressions of punching shear capacity from EN 1992-1-1:2023[55] also provided a reasonable level of accuracy, comparable to that of the one-way shear expressions, indicating a close correlation between one-way and two-way shear resistance expressions in the current code.

7 | CONCLUSIONS

In this study, the one-way and two-way shear capacities of one-way slabs under concentrated loads were evaluated using the CSCT expressions and LEFEA. Different support conditions were addressed, including simply SSs, cantilever slabs, and continuous slabs. Besides evaluating the shear and punching shear capacity, the predictions of the governing failure mechanism were also discussed. At the end, the following conclusions can be drawn:

- The coupling of the CSCT with LEFEA allows for predicting the shear and punching capacity of most one-way slabs under concentrated loads in non-axis-symmetrical conditions accurately. However, it is clear that the one-way shear approach provides better levels of accuracy, even when the test fails due to punching shear. This occurs because the failure is almost always triggered locally around the load on the most heavily loaded side.
- The punching shear capacity approach allows predicting accurately the capacity of the tests that are critical in punching. Besides, the introduction of the correction factor β_{width} allowed for improving the predictions of load capacity, even when the tests failed by one-way shear, by considering the transition between two-way shear and one-way shear when the slab width decreases.
- Comparing the predicted loads to cause the one-way shear failure and punching shear failure, it is possible to determine the governing failure mechanism of the tests in more than 70%, regardless of the boundary conditions of the slabs. When the correct governing failure mechanism is not predicted, a conservative prediction of ultimate capacity occurs under reasonable levels.
- The use of fully analytical approaches grounded on the current EN 1992-1-1:2023[55] may also provide excellent levels of accuracy if a proper definition of effective shear width may be applied, such as the one suggested by Halvonik et al.[6] in one-way shear predictions. Compared to the proposed approach, combining LEFEA and CSCT expressions, the use of EN 1992-1-1:2023 tends to provide slightly more conservative predictions,

which will be adequate for preliminary assessment of a large number of slabs.

Therefore, LEFEA can be employed together with the CSCT expressions to achieve enhanced levels of accuracy in the assessments of existing bridge deck slabs. In practice, the presented approach allows for reaching similar levels of accuracy to those using non-linear finite element analyses,[57] but without expending significant time in the calibration of the numerical models.

ACKNOWLEDGMENTS

This research was funded by the São Paulo Research Foundation (FAPESP) (grant number 2024/13561-5); São Paulo State University (UNESP) EDITAL 03/2025 PROPe (Programa de Incentivo e Estímulo à Pesquisa aos Recém-contratados—IEPe-RC); and the Article Processing Charge for the publication of this research was funded by the Coordenação de Aperfeiçoamento de Pessoal de Nível Superior—Brasil (CAPES)—Finance Code 001 (ROR identifier: 00x0ma614). The Article Processing Charge for the publication of this research was funded by the Coordenação de Aperfeiçoamento de Pessoal de Nível Superior - Brasil (CAPES) (ROR identifier: 00x0ma614).

DATA AVAILABILITY STATEMENT

The data that support the findings of this study are available from the corresponding author upon reasonable request.

ORCID

Mounir Khalil El Debs https://orcid.org/0000-0001-5955-7936

REFERENCES

1. Natário F, Fernández Ruiz M, Muttoni A. Shear strength of RC slabs under concentrated loads near clamped linear supports. Eng Struct. 2014;76:10–23. https://doi.org/10.1016/j.engstruct.2014.06.036
2. Lantsoght EOL, van der Veen C, Walraven JC, de Boer A. Transition from one-way to two-way shear in slabs under concentrated loads. Mag Concr Res. 2015;67:909–22. https://doi.org/10.1680/macr.14.00124
3. de Sousa AMD, Lantsoght EOL, Yang Y, El Debs MK. Extended CSDT model for shear capacity assessments of bridge deck slabs. Eng Struct. 2021;234:111897. https://doi.org/10.1016/j.engstruct.2021.111897
4. Shu J. Shear assessment of a reinforced concrete bridge deck slab according to level-of-approximation approach. Struct Concr. 2018;19:1838–50. https://doi.org/10.1002/suco.201700283
5. Henze L, Rombach GA, Harter M. New approach for shear design of reinforced concrete slabs under concentrated loads based on tests and statistical analysis. Eng Struct. 2020;219:110795. https://doi.org/10.1016/j.engstruct.2020.110795
6. Halvonik J, Vidaković A, Vida R. Shear capacity of clamped deck slabs subjected to a concentrated load. J Bridg Eng. 2020;25:04020037. https://doi.org/10.1061/(ASCE)BE.1943-5592.0001564
7. Lantsoght EOL, de Boer A, van der Veen C, Walraven JC. Effective shear width of concrete slab bridges. Bridge Eng. 2015;168:287–98. https://doi.org/10.1680/bren.13.00027
8. Lantsoght EOL, van der Veen C, de Boer A, Walraven JC. Transverse load redistribution and effective shear width in reinforced concrete slabs. Heron. 2015;60:145–79.
9. Belletti B, Damoni C, Hendriks MAN, De Boer A. Analytical and numerical evaluation of the design shear resistance of reinforced concrete slabs. Struct Concr. 2014;15:317–30. https://doi.org/10.1002/suco.201300069
10. Natário F. Static and fatigue shear strength of reinforced concrete slabs under concentrated loads near linear support. PhD Thesis (Docteur ès Sciences). Lausanne, Switzerland: École Polytechnique Fédérale de Lausanne (EPFL); 2015. https://doi.org/10.5075/epfl-thesis-6670
11. Reißen K, Classen M, Hegger J. Shear in reinforced concrete slabs-experimental investigations in the effective shear width of one-way slabs under concentrated loads and with different degrees of rotational restraint. Struct Concr. 2018;19:36–48. https://doi.org/10.1002/suco.201700067
12. de Sousa AMD, Lantsoght EOL, El Debs MK. Transition between shear and punching in reinforced concrete slabs: review and predictions with ACI code expressions. ACI Struct J. 2023;120:115–28. https://doi.org/10.14359/51738350
13. de Sousa AMD, Lantsoght EOL, El Debs MK. Shear and punching capacity predictions for one-way slabs under concentrated loads considering the transition between failure mechanisms. Buildings. 2023;13:13. https://doi.org/10.3390/buildings13020434
14. Muttoni A, Fernandez Ruiz M. Shear strength of members without transverse reinforcement as function of critical shear crack width. ACI Struct J. 2008;105:163–72. https://doi.org/10.14359/19731
15. Muttoni A. Punching shear strength of reinforced concrete slabs without transverse reinforcement. ACI Struct J. 2008;105:440–50. https://doi.org/10.14359/19858
16. Muttoni A, Schwartz J. Behavior of beams and punching in slabs without shear reinforcement. IABSE Colloquium. 1991;62:703–8.
17. Kani GNJ. The riddle of shear failure and its solution. ACI J Proc. 1964;61:441–68. https://doi.org/10.14359/7791
18. Walraven JC. Fundamental analysis of aggregate interlock. J Struct Div ASCE. 1981;107:2245–70.
19. Dulacska H. Dowel action of reinforcement crossing cracks in concrete. ACI J Proc. 1972;69:754–7. https://doi.org/10.14359/11281
20. Taylor HP Investigation of the dowel shear forces carried by the tensile steel in reinforced concrete beams Cement and Concrete Association 1969.
21. Vecchio FJ, Collins MP. The modified compression-field theory for reinforced concrete elements subjected to shear. ACI J Proc. 1986;83:219–31. https://doi.org/10.14359/10416
22. FD P 18-717. Eurocode 2—Calcul des structures en béton—Guide d'application des normes NF EN 1992. 2013.
23. Westergaard HM. Computation of stresses in bridge slabs due to wheel loads. Public Roads. 1930;11:1–23.

24. Belletti B, Scolari M, Muttoni A, Cantone R. Shear strength evaluation of RC bridge deck slabs according to CSCT with multilayered shell elements and PARC_CL crack model. Geneva, Switzerland: IABSE Conference Geneva; 2015. p. 1158–65.
25. Lantsoght EOL, de Boer A, van der Veen C. Distribution of peak shear stress in finite element models of reinforced concrete slabs. Eng Struct. 2017;148:571–83. https://doi.org/10.1016/j.engstruct.2017.07.005
26. de Sousa AMD, Lantsoght EOL, Setiawan A, El Debs MK. Shear and punching capacity predictions for slabs under concentrated loads aided by LEFEA. SP-357: punching shear of concrete slabs: insights from new materials, tests, and analysis methods. Volume 357. Farmington Hills, MI: American Concrete Institute; 2023. p. 100–22. https://doi.org/10.14359/51738762
27. Sagaseta J, Muttoni A, Ruiz MF, Tassinari L. Non-axis-symmetrical punching shear around internal columns of RC slabs without transverse reinforcement. Mag Concr Res. 2011;63:441–57. https://doi.org/10.1680/macr.10.00098
28. Sagaseta J, Tassinari L, Fernández Ruiz M, Muttoni A. Punching of flat slabs supported on rectangular columns. Eng Struct. 2014;77:17–33. https://doi.org/10.1016/j.engstruct.2014.07.007
29. Fédération Internationale du Béton (fib). fib Model Code for Concrete Structures 2010. vol. 1–2. Lausanne, Switzerland: Ernst & Sohn - fédération internationale du béton, Bulletin 65; 2012.
30. Setiawan A, Vollum RL, Macorini L, Izzuddin BA. Punching shear design of RC flat slabs supported on wall corners. Struct Concr. 2020;21: 1548–65. https://doi.org/10.1002/suco.201900514
31. Setiawan A, Vollum RL, Macorini L, Izzuddin BA. Punching of RC slabs without transverse reinforcement supported on elongated columns. Structure. 2020;27:2048–68. https://doi.org/10.1016/j.istruc.2020.08.017
32. Cavagnis F, Fernández Ruiz M, Muttoni A. A mechanical model for failures in shear of members without transverse reinforcement based on development of a critical shear crack. Eng Struct. 2018;157:300–15. https://doi.org/10.1016/j.engstruct.2017.12.004
33. Setiawan A, Cantone R, Fernández Ruiz M, Muttoni A. Verification of shear failures of cantilever bridge deck slabs subjected to concentrated loads. Eng Struct. 2024;303:117491. https://doi.org/10.1016/j.engstruct.2024.117491
34. Vaz Rodrigues R, Fernández Ruiz M, Muttoni A. Shear strength of R/C bridge cantilever slabs. Eng Struct. 2008;30:3024–33. https://doi.org/10.1016/j.engstruct.2008.04.017
35. de Sousa A, Lantsoght E, Setiawan A, El Debs M. Transition from one-way to two-way shear by coupling LEFEA and the CSCT models. Proceedings of the Fib Symposium 2021, Concrete Structures: New Trends for Eco-Efficiency and Performance. 2021.
36. Reißen K. Zum Querkrafttragverhalten von einachsig gespannten Stahlbe-tonplatten ohne Querkraftbewehrung unter Einzellasten. Doctor of Engineering. PhD Thesis (Doctor of Engineering), Faculty of Civil Engineering, RWTH Aachen University. 2016.
37. de Sousa AMD, Lantsoght EOL, El Debs MK. Failure mechanism of one-way slabs under concentrated loads after local reinforcement yielding. Eng Struct. 2023;291:116396. https://doi.org/10.1016/j.engstruct.2023.116396
38. de Sousa AMD, Lantsoght EOL, El Debs MK. One-way shear strength of wide reinforced concrete members without stirrups. Struct Concr. 2020;22(2):1. https://doi.org/10.1002/suco.202000034
39. de Alex MDS. Database of tests evaluated with the combination of LEFEA and CSCT expressions. Zenodo. 2026. https://doi.org/10.5281/zenodo.17940106
40. Damasceno LSR. Experimental analysis of one-way reinforced concrete flat slabs in punching shear with rectangular columns (in Portuguese: Análise experimental de lajes lisas unidirecionais de concreto armado com pilares retangulares ao puncionamento). Belém, PA, Brazil: Masters' thesis, Departamento de Engenharia Civil, Universidade Federal do Pará,; 2007. https://doi.org/10.1038/ni.2454
41. de Ferreira MP. Experimental analysis of one-way reinforced concrete flat slabs in axis or non-axis-symmetric punching shear (in Portuguese: Análise experimental de lajes lisas unidirecionais de concreto armado ao puncionamento simétrico ou assimétrico). Masters' thesis, Universidade Federal do Pará. 2006.
42. de Ferreira MP, Sacramento PVP, Lima Neto AF, Teixeira MR, de Oliveira DRC. Punching strength of RC slabs with asymmetric point loads. Acta Sci Technol. 2016;38:71–80. https://doi.org/10.4025/actascitechnol.v38i1.27305
43. Regan PE, Rezai-Jorabi H. Shear resistance of one-way slabs under concentrated loads. ACI Struct J. 1988;85:150–7. https://doi.org/10.14359/2704
44. Oliveira DRC, Regan PE, Melo GSSA. Punching resistance of RC slabs with rectangular columns. Mag Concr Res. 2004;56:123–38. https://doi.org/10.1680/macr.2004.56.3.123
45. Rombach G, Henze L. Querkrafttragfähigkeit von Stahlbetonplatten ohne Querkraftbewehrung unter konzentrierten Einzellasten. Beton Und Stahlbetonbau. 2017;112:568–78. https://doi.org/10.1002/best.201700040
46. Natário F, Fernández Ruiz M, Muttoni A. Experimental investigation on fatigue of concrete cantilever bridge deck slabs subjected to concentrated loads. Eng Struct. 2015;89:191–203. https://doi.org/10.1016/J.ENGSTRUCT.2015.02.010
47. Rombach GA, Latte S. Shear resistance of bridge decks without shear reinforcement. In: Walraven JC, Stoelhorst D, editors. Proceedings of the International fib Symposium, Amsterdam, The Netherlands, 19–21 May 2008. London: Taylor & Francis Group; 2008. p. 519–25. https://doi.org/10.1201/9781439828410.ch86
48. Rombach G, Latte S. Querkrafttragfähigkeit Von Fahrbahnplatten Ohne Querkraftbewehrung. Beton Und Stahlbetonbau. 2009;104:642–56. https://doi.org/10.1002/best.200900029
49. Vida R, Halvonik J. Experimentálne overovanie šmykovej odolnosti mostovkových dosiek (Experimental verification of shear resistance of bridge deck slabs). Bratislava, Slovakia: Inžinierske Stavby/Inženýrské Stavby,; 2018. p. 2–6.
50. Lantsoght EOL, van der Veen C, Walraven J, de Boer A. Recommendations for the shear assessment of reinforced concrete slab bridges from experiments. Struct Eng Int. 2013;23:418–26. https://doi.org/10.2749/101686613X13627347100239
51. Lantsoght EOL, van der Veen C, Koekkoek R, Sliedrecht H. Punching capacity of prestressed concrete bridge decks under

fatigue. ACI Struct J. 2019;116:209–18. https://doi.org/10.14359/51715563
52. DIN EN 1992-2/NA. National Annex—Nationally determined parameters - Eurocode 2: Design of concrete structures—Part 2: Concrete bridges - Design and detailing rules. 2013.
53. ABNT NBR 6118. NBR 6118: design of concrete structures — procedure (in portuguese). Rio de Janeiro: Associação Brasileira de Normas Técnicas (ABNT); 2014.
54. Lantsoght EOL, van der Veen C, Walraven JC. Shear in one-way slabs under concentrated load close to support. ACI Struct J. 2013;110:275–84. https://doi.org/10.14359/51684407
55. European Committee for Standardization. Eurocode 2: design of concrete structures. Part 1–1: general rules and rules for building, bridges and other civil engineering structures. Brussels, Belgium: CEN; 2023.
56. Lantsoght EOL, van der Veen C, Walraven JC, de Boer A. Database of wide concrete members failing in shear. Mag Concr Res. 2015;67:33–52. https://doi.org/10.1680/macr.14.00137
57. de Sousa AMD, Lantsoght EOL, Genikomsou AS, Prado LP, El Debs MK. NLFEA of one-way slabs in transition between shear and punching: recommendations for modeling. Eng Struct. 2023;293:116617. https://doi.org/10.1016/j.engstruct.2023.116617

AUTHOR BIOGRAPHIES

Alex Micael Dantas de Sousa Assistant Professor, School of Engineering, São Paulo State University (UNESP), Ilha Solteira, Brazil. Email: alex.dantas@unesp.br

Eva Olivia Leontien Lantsoght Vice Dean for Research, Decanato de Investigación, Universidad San Francisco de Quito (USFQ), Quito, Ecuador. Email: elantsoght@usfq.edu.ec

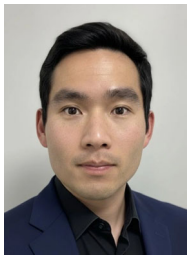

Andri Setiawan Postdoctoral fellow, Instituto de Ciencia y Tecnología del Hormigón (ICITECH), Universitat Politècnica de València (UPV), Valencia, Spain. Email: asetiaw1@upvnet.upv.es

Mounir Khalil El Debs Senior Professor, São Carlos School of Engineering (EESC), University of São Paulo (USP), São Carlos, Brazil. Email: mkdebs@sc.usp.br

How to cite this article: de Sousa AMD, Lantsoght EOL, Setiawan A, El Debs MK. Failure mechanism and resistance predictions for one-way slabs in transition between shear and punching coupling linear elastic finite element analyses with critical shear crack theory-based models. Structural Concrete. 2026. https://doi.org/10.1002/suco.70546

APPENDIX A

PROPOSED APPROACH FOR FULLY ANALYTICAL VERIFICATION WITH EN 1992-1-1:2023[55]

A.1 | One-way shear

In this study, we proposed that the following expression shall be used to predict the one-way shear capacity for fully analytical predictions with EN 1992-1-1:2023[55]:

$$V_{R,EC23} = \left(\frac{\tau_{R,c}}{\beta_{shear}}\right) \cdot b_{eff,analytical} \cdot d \tag{A1}$$

Using the average values of material properties and unitary partial safety factors for the comparison between tested and predicted resistances, the shear strength $\tau_{R,c}$ should be taken as:

$$\tau_{R,c} = \frac{0.66}{\gamma_v} \cdot \left(100 \cdot \rho_l \cdot f_{cm} \cdot \frac{d_{dg}}{d}\right)^{1/3} \geq \tau_{R,\min} \tag{A2}$$

$$\tau_{R,\min} = \frac{11}{\gamma_v} \cdot \sqrt{\frac{f_{cm}}{f_{ym}} \cdot \frac{d_{dg}}{d}} \tag{A3}$$

where:

γ_v is the partial factor for shear design; f_{ck} is the characteristic concrete cylinder compressive strength; f_{yd} is the design value of the yield strength, which has been used to design the flexural reinforcement; d is the

effective depth of the flexural reinforcement. d_{dg} is a size parameter describing the failure zone roughness, which depends on the concrete type and its aggregate properties, which may be taken as:

$$d_{dg} = \begin{cases} 16\,\text{mm} + D_{lower} \le 40\,\text{mm}, \text{if } f_{ck} \le 60MPa \\ 16\,\text{mm} + D_{lower} \cdot (60/f_{ck})^2 \le 40\,\text{mm}, \text{for } f_{ck} > 60MPa \end{cases} \quad \text{(A4)}$$

D_{lower} is the smallest value of the upper sieve size D in an aggregate for the coarsest fraction of aggregates in the concrete permitted by the specification of concrete[52]; ρl is the reinforcement ratio for bonded longitudinal reinforcement in the tensile zone due to bending referred to the nominal concrete area ($= A_{sl}/b_w \cdot d$); A_{sl} is the effective area of tensile reinforcement at the distance d beyond the section considered; b_w is the width of the cross-section of linear members.

The effective shear width can be estimated as suggested by Halvonik et al.[6] as:

$$b_{eff,analytical} = \min \begin{cases} l_{load} + 2 \cdot (b_{load} + 2 \cdot a_v) \\ l_{load} + 2 \cdot (b_{load} + 2 \cdot d) \end{cases} \quad \text{(A5)}$$

$$\beta_{shear} = \frac{a_v}{2.75 \cdot d_l}, \text{with } d_l \le a_v \le 2.75 d_l \quad \text{(A6)}$$

A.2 | Two-way shear

The punching shear capacity, when using the new Eurocode expressions, can be estimated as:

$$P_{R,EC23} = \left(\frac{\tau_{R,c}}{\beta_{shear}}\right) \cdot b_{0,x1} \cdot d_v + \tau_{R,c} \cdot b_{0,x2} \cdot d_v + \tau_{R,c} \cdot b_{0,y1} \cdot d_v + \tau_{R,c} \cdot b_{0,y2} \cdot d_v \quad \text{(A7)}$$

On which the shear strength $\tau_{R.c}$ (in stress units) is calculated as:

$$\tau_{R,c} = \frac{0.6}{\gamma_v} \cdot k_{pb} \cdot \left(100 \cdot \rho_l \cdot f_{cm} \cdot \frac{d_{dg}}{d_v}\right)^{1/3} \le \frac{0.5}{\gamma_v}\sqrt{f_{cm}} \quad \text{(A8)}$$

where:

$$\rho_l = \sqrt{\rho_{l,x} \cdot \rho_{l,y}} \quad \text{(A9)}$$

$\rho_{l.x}$ and $\rho_{l.y}$ are reinforcement ratios of bonded flexural reinforcement in the x- and y-directions, respectively. d_{dg} is defined as in Equation (A4); k_{pb} is the punching shear gradient enhancement coefficient that may be calculated as:

$$k_{pb} = 3.6\sqrt{1 - \frac{b_0}{b_{0,5}}}, \text{with } 1 \le k_{pb} \le 2.5 \quad \text{(A10)}$$

b_0 is the length of the perimeter at the face of the supporting area and $b_{0,5}$ is the length of the total control perimeter.